

ESA CREST – Climate data Record of Stratospheric aerosols

ESA - 4000130839/20/I-DT

Final Report

Version: 1.4 (5 December 2022)
Distribution: C. Retscher (ESA) and the CREST team (FMI, UB)
Prepared by: A. Rozanov, V. Sofieva, M. Szlag

Contents

1	Summary	3
2	Introduction	3
3	The workpackage (WP) results	4
3.1	WP 1. Feasibility of the retrieval of the stratospheric aerosol extinction coefficient at 525 nm from limb-scatter measurements	4
3.2	WP 2. Methods to convert the aerosol extinction coefficient to different wavelength.....	6
3.3	WP3. Improvement of the OMPS stratospheric aerosol extinction time series.....	14
3.4	WP 4. New data set of aerosol extinction coefficient from GOMOS stellar occultation measurements	24
3.4.1	Introduction: motivation for the study.....	24
3.4.2	The inversion algorithm	25
3.4.3	Retrieval results and intercomparisons	28
3.4.4	GOMOS aerosol climate data record	31
3.4.5	Conclusions	34
3.5	WP 5. CDR of stratospheric aerosols.....	34
3.5.1	Merged dataset of aerosol profiles	34
3.5.2	Filling gaps in SAGE II data during Pinatubo	40
3.5.3	Creating stratospheric aerosol optical depth (SAOD).....	41
3.5.4	The merged CREST SAOD dataset: illustrations, comparison with GLOSSAC....	42

3.5.5	Summary	44
3.6	WP6. Application: influence of the volcanic activity on long-term ozone trends	45
4	Datasets and data access	47
5	Main results and useful future work	49

1 Summary

Stratospheric aerosols impact the radiative forcing and thus the energy balance of the Earth's atmosphere, therefore information about their distribution and variability is of high importance for climate related studies. The main scientific objective of the project CREST is creating a new merged long-term time series of the vertically resolved aerosol extinction coefficients using data records from SAGE II, OSIRIS, GOMOS, SCIAMACHY and OMPS-LP instruments for the years from 1984 to present.

In the project, we have performed various feasibility studies related to improvement of aerosol retrievals from the individual satellite datasets, as well as related to the developing optimal methods for merging time series of aerosol extinction coefficients at different wavelengths. New versions of SCIAMACHY (UBr v3.0) and OMPS-LP (UBr v1.2) aerosol extinction profile data sets have been created. A new GOMOS multi-wavelength (400 – 750 nm) aerosol extinction profile dataset (FMI GOMOS-Aero v 1.0), which is based on retrievals from averaged GOMOS transmittances in dark-limb occultations, has been developed. These new aerosol datasets have improved data quality.

The merged dataset of vertically resolved stratospheric aerosol extinction coefficients is derived from data by six limb and occultation satellite instruments: SAGE II on ERBS, GOMOS and SCIAMACHY on Envisat, OSIRIS on Odin, OMPS on Suomi-NPP, and SAGE III on International Space Station. The merging of aerosol profiles is performed by transformation of the aerosol datasets from individual satellite instruments to the same wavelength, i.e., 750 nm, and their de-biasing and homogenization by adjusting the seasonal cycles. The merged aerosol extinction coefficient is computed as the median of the adjusted data from the individual instruments. The merged time series of vertically resolved monthly mean aerosol extinction coefficients at 750 nm is provided in 10° latitudinal bins from 90°S to 90°N, in the altitude range from 8.5 km to 39.5 km. The time series of the stratospheric aerosol optical depth (SAOD) is created by integration of aerosol extinction profiles from the tropopause to 39.5 km; it is also provided as monthly mean data in 10° latitudinal bins. The created aerosol climate record covers the period from October 1984 until May 2022, and it is intended to be extended in the future.

2 Introduction

The main scientific objective of the project is creating a new merged long-term time series of aerosol extinction coefficients using data records from SAGE II, OSIRIS, GOMOS, SCIAMACHY and OMPS-LP instruments for the years 1984-present.

The specific objectives include:

- Improvement of the quality of the existing aerosol extinction data sets from GOMOS and OMPS-LP
- Development of methods to reduce the uncertainty when merging time series of aerosol extinction coefficients at different wavelengths.

- Demonstrating the application of the new merged aerosol dataset in climate-related studies (ozone trends are considered as an example)

The report is organized as follows: Section 3 contains the results of the project works specified in work packages. Section 4 is dedicated to the description of the merged stratospheric aerosol datasets and data access. Main results and future useful works are discussed in Section 5.

3 The work package (WP) results

3.1 WP 1. Feasibility of the retrieval of the stratospheric aerosol extinction coefficient at 525 nm from limb-scatter measurements

A direct retrieval of the aerosol extinction coefficient from limb-scatter observations at 525 nm would be a straightforward way to avoid errors associated with a transformation of the aerosol extinction coefficient to another wavelength when merging data sets from different instruments. Although it is generally accepted that limb-scatter retrievals at shorter wavelengths have less sensitivity, no quantitative results have been published so far. In this work package we investigated the accuracy of SCIAMACHY retrievals at 525 nm to check if these would provide better accuracy (although it is expected to be less than that of 750 nm retrieval) than that of the results converted from 750 nm.

First, a theoretical investigation of the retrieval characteristics was performed analyzing the averaging kernels of the retrieval. As the averaging kernels depend on the extinction profile assumed in the model, the values based on the a priori profile were considered. As each retrieval is initialized with the same a priori profile and thus characterized by the same averaging kernel, i.e., the initial sensitivity is similar for all measurements (might, however somewhat vary for different viewing geometries).

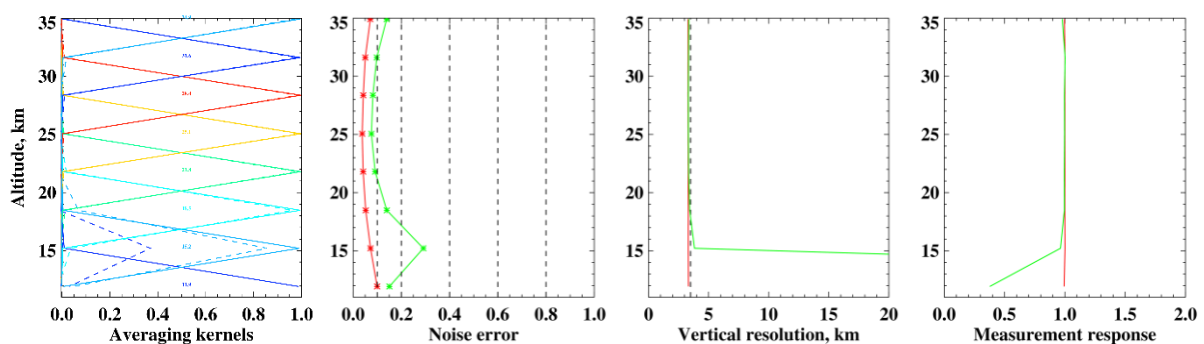


Figure 1. Retrieval characteristics (from left to right): averaging kernels (solid line for 750 nm, dashed line for 525 nm), retrieval noise error, vertical resolution and measurement response (red for 750 nm, green for 525 nm).

Figure 1 shows retrieval characteristics for a selected tropical measurement, which are considered to be representative for all tropical observations. The averaging kernels shown in the left panel of the plot illustrate degrading sensitivity at 12 km for 525 nm retrievals (dashed lines) in comparison to those at 750 nm (solid lines). For 525 nm retrievals, the peak of the 12 km averaging kernel is displaced to 15 km and its amplitude is reduced to 0.4. At 15 km, the

averaging kernel for 525 nm retrieval has a peak at the nominal altitude but a lower amplitude than that of the 750 nm retrieval. The noise error, shown in the second panel from the left, is larger for 525 nm (green line) than for 750 nm (red line) throughout the whole altitude range. The vertical resolution of the 525 nm retrieval is slightly coarser than that of the 750 nm down to 15 km and rapidly degrades below. A similar behavior is observed for the measurement response shown in the right panel of the plot. At 525 nm, the measurement response is slightly below 1 at 15 km and degrades to 0.4 at 12 km. Overall, it is expected from the theoretical studies, that the retrieval at 525 nm will have somewhat reduced sensitivity at 15 km and is not sensitive enough at 12 km anymore.

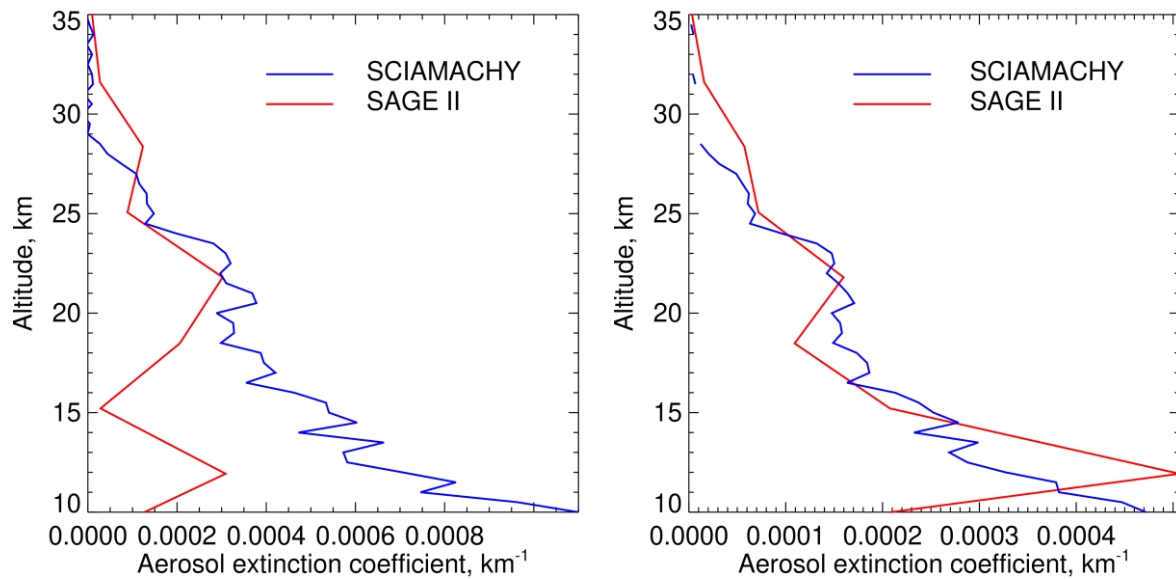


Figure 2. Comparison of the aerosol extinction coefficients retrieved from SCIAMACHY limb measurements at wavelengths of 525 nm (left panel) and 750 nm (right panel) with results for SAGE II instrument.

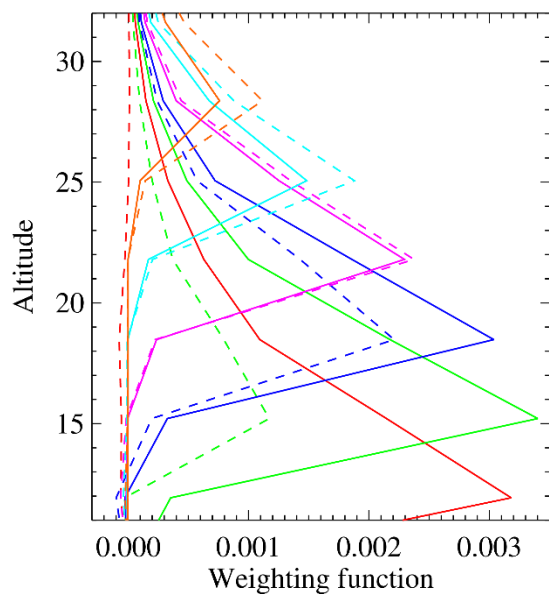


Figure 3. Weighting functions of the limb-scatter retrieval at 750 nm (solid line) and 525 nm (dashed line).

To illustrate the results from real retrievals we show comparisons of SCIAMACHY results using the measurements at 525 and 750 nm with the results from SAGE II for one selected measurement in Figure 2. The observed behavior is found to be typical for most of the tropical profiles. While a good agreement with SAGE II data is obtained for the retrieval at 750 nm, shown in the right panel of the plot, the retrieval at 525 nm loses its performance already below 18 km producing unrealistically small values at 15 km. The observed behavior can be understood by analyzing the weighting functions of the aerosol extinction coefficient at 750 and 525 nm as shown in Figure 3 by solid and dashed lines, respectively. It is seen that at 750 nm the weighting function at 12 km has a pronounced peak with nearly the same amplitude as for 15

km while the weighting function at 525 nm is almost zero, which determines the lack of sensitivity at 12 km at this wavelength. At 15 km altitude, the weighting function at 525 nm has already a pronounced maximum providing a sensitivity to the retrieval, but the amplitude of the peak is much lower compared to that at 750 nm. The consequence of the much smaller weighting function is a higher sensitivity to errors in the measured/modeled radiance profile as e.g., measurement noise or wrong assumption about the aerosols at the reference tangent height. This determines the instability of real retrievals. With increasing altitude, the weighting functions at 525 nm are getting closer to those at 750 nm and even exceeding them above 25 km, which ensures comparable retrieval results above 18 km.

In the light of the findings presented above, the direct retrieval of the aerosol extinction coefficient from limb-scatter observations at a wavelength of 525 nm is considered unfavorable.

3.2 WP 2. Methods to convert the aerosol extinction coefficient to different wavelength

To optimize the method to convert the aerosol extinction coefficient between different wavelengths, we first analyze the error associated with the conversion from 750 nm (OSIRIS, SCIAMACHY) to 525 nm (SAGE II) assuming a fixed particle size distribution as it is done, e.g., in the version 1.0 of the GloSSAC climatology (Thomason et al., 2018). To this end we use the tropical data set of the stratospheric aerosol particle size distribution (PSD) retrieved from SCIAMACHY limb-scatter measurements (Malinina et al., 2018). All data from August 2002 to April 2012 are used. First, data sets at 525 and 750 nm are calculated employing the Mie theory with PSD values from SCIAMACHY database. The former is considered to be the reference data set while the latter is converted to 525 nm using the Ångström exponent approximation. The Ångström exponent is calculated from the aerosol extinction coefficients calculated at 525 and 750 nm employing the Mie theory and assuming a fixed log-normal particle size distribution with the mode radius of 0.08 μm and sigma of 1.6.

The conversion errors were investigated for the aerosol extinction coefficient itself and for its relative and absolute anomalies. The results are presented in Figure 4 with the extinction coefficient (top panel) and its relative (middle panel) and absolute (bottom panel) anomalies shown in the left panels of the plot and the corresponding differences shown in the right panels. While the relative differences are shown for the extinction coefficient, the absolute differences are presented for both anomalies. In the left panels the reference data set obtained from the Mie calculations is shown in red while the approximate data set calculated using the Ångström exponent is shown in blue.

It is seen from the plot that the relative difference for the extinction coefficient varies from -15 to 20%, shows a pronounced seasonal variation and increases with increasing stratospheric aerosol level after 2006. The differences for the relative and absolute anomalies behave similarly, changing from negative to predominantly positive values after 2006. As a measure of the discrepancies between the anomalies, the standard deviation of the difference time series divided by the standard deviation of the reference anomaly time series and multiplied by 100% is used. This results in 16% difference for the relative anomaly and 22% difference for the absolute anomaly.

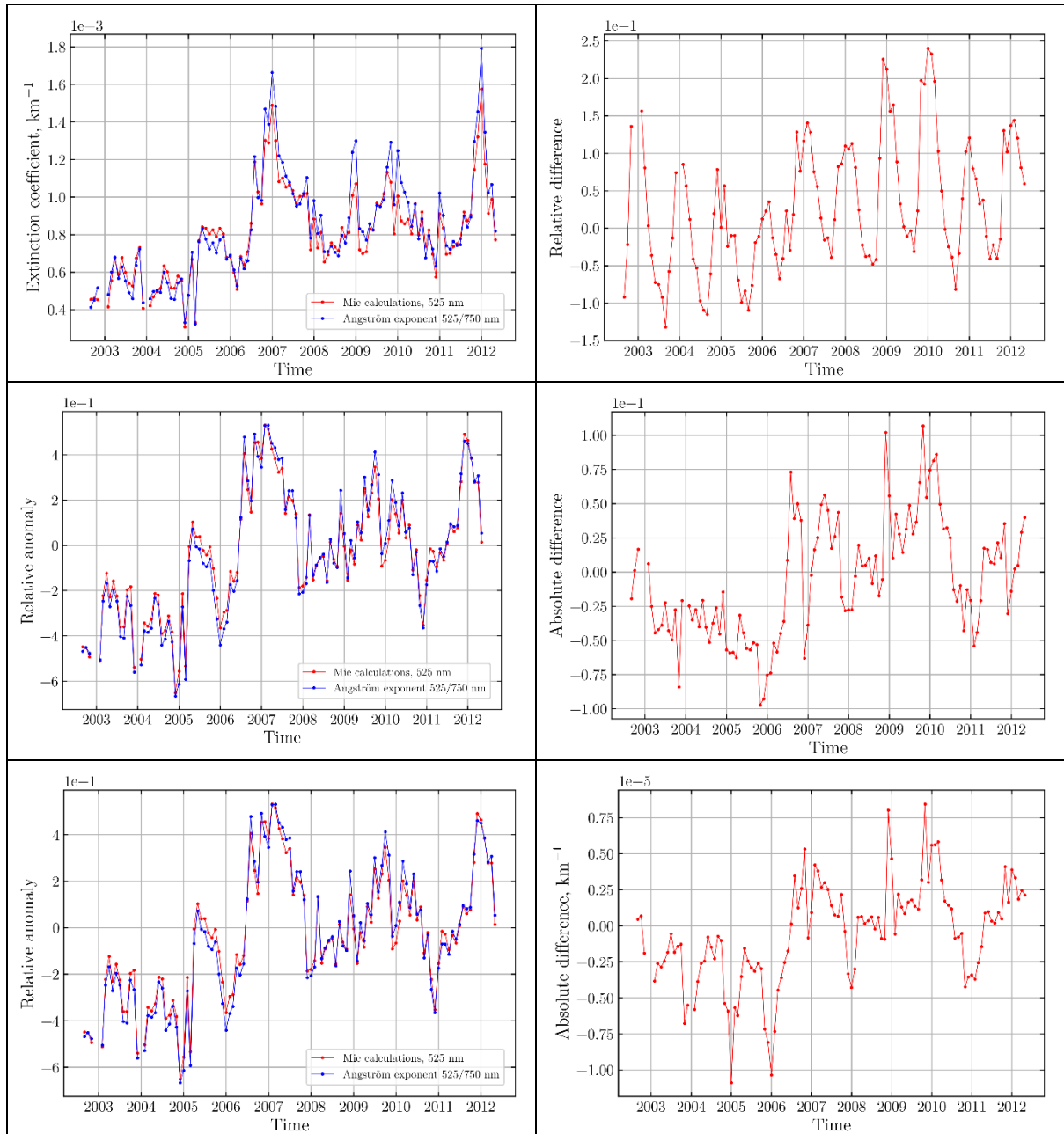


Figure 4. Error associated with the conversion of the extinction coefficient from 750 nm to 525 nm assuming a fixed particle size distribution. The left panels show the aerosol extinction coefficient (top), relative anomaly of the extinction coefficient (bottom) and absolute anomaly of the extinction coefficient (bottom). The result obtained with exact Mie calculations are shown in red, while the approximation by the Ångström exponent is depicted by blue. Differences between the results obtained using the Ångström exponent conversion and Mie calculations are shown in the right panels

As a next step, correlations of the errors in the converted aerosol extinction coefficient with different parameters of the aerosol particle size distribution and with the aerosol extinction coefficient itself were considered. The results are presented in Figure 5. The dependence of the error on the mode radius of the aerosol PSD shown in the top left panel of the plot does not show any reasonable correlation. On the contrary, a high correlation is observed for the dependence of the error on the distribution width, which is defined as the standard deviation of the PSD: $w = \sqrt{R_{med}^2 e^{\sigma}(e^{\sigma} - 1)}$. This demonstrates that the width of the PSD has a

predominant influence on the resulting value of the Ångström exponent. Similar, but somewhat weaker correlation is obtained for the effective radius, as defined by $R_{eff} = R_{med} \exp(5 \ln(\sigma)^2 / 2)$, see the lower right panel of the plot. Surprisingly low (almost absent) is the correlation between the conversion error and the aerosol extinction coefficient itself. This finding is unexpected as larger differences from the assumed fixed PSD are expected during periods of high volcanic activities, where also increased values of the extinction are expected. The obtained results demonstrate, however, that no extinction-based climatology can be established to make the wavelength conversion more accurate.

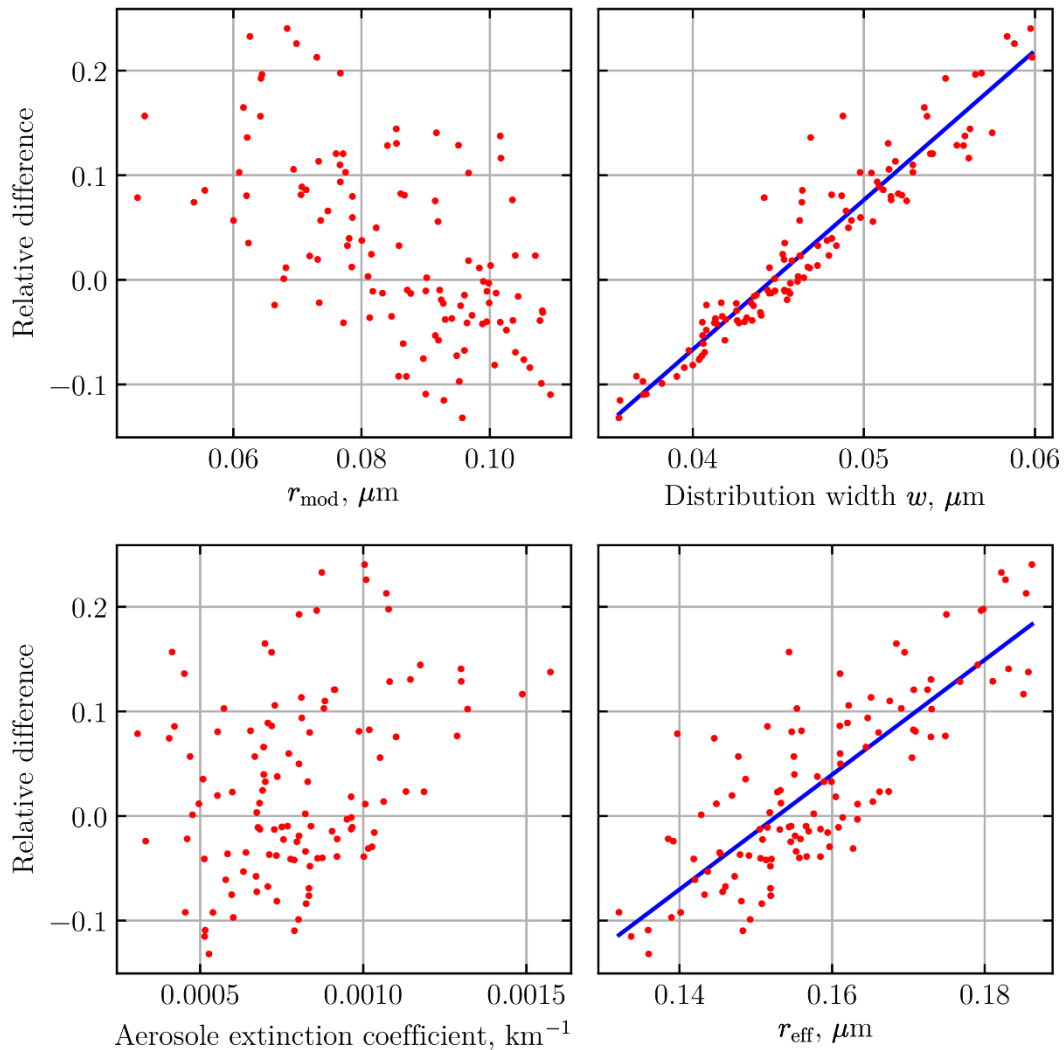


Figure 5. Correlation between the relative errors in the aerosol extinction coefficients and the aerosol particle size distribution parameters as well as aerosol extinction coefficient itself.

After analyzing all aerosol data sets intended to be included in the merged data set, an alternative strategy to minimize the uncertainties associated with the conversion of the aerosol extinction coefficient between different wavelengths can be suggested. As no instruments providing the information on either the Ångström exponents or aerosol particle size distribution parameters during the entire operation time of OMPS-LP instrument are available, it seems advantageous to select one of the wavelengths, at which the aerosol extinction coefficients from OMPS-LP are available, as the main wavelengths to create the

aerosol record. The selection of the optimal wavelength(s) is dealt with later within WP3. The SAGE II data can be converted to this/these wavelength(s) using the 525/1020 nm Ångström exponent. Both SCIAMACHY and OSIRIS can be converted using a fixed aerosol particle size distribution (PSD) assumption or 400/675 nm Ångström exponent from GOMOS. However, some other assumptions need to be used to convert between 750 nm wavelength of OSIRIS and the wavelength(s) of OMPS-LP between 2012 (end of ENVISAT mission) and 2017 (start of SAGE III/ISS mission).

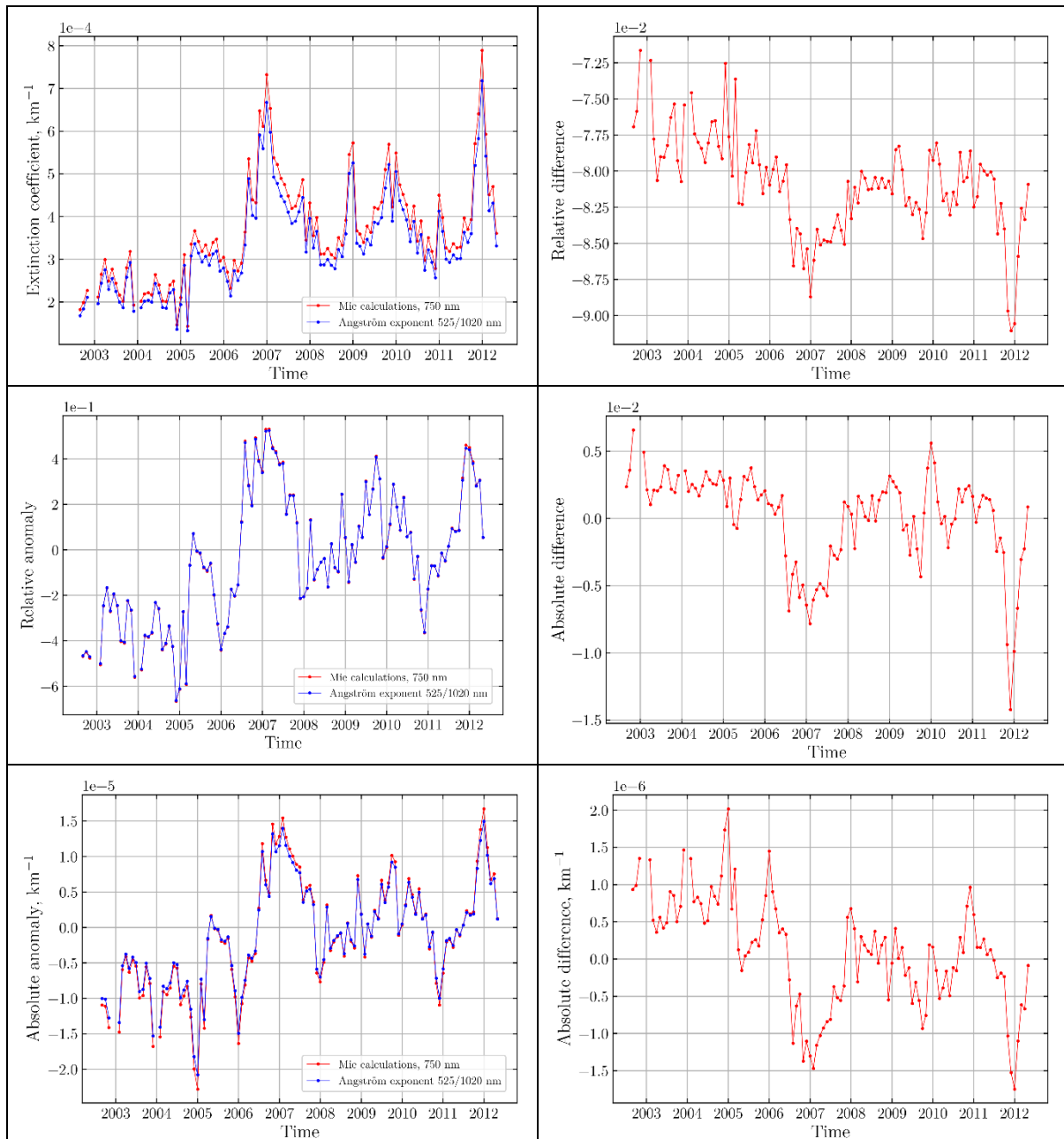


Figure 6. Error associated with the conversion of the aerosol extinction coefficient from SAGE II wavelengths to 750 nm using the Ångström exponent calculated for the wavelengths of 525 and 1020 nm. The left panels show the aerosol extinction coefficient (top), relative anomaly of the extinction coefficient (middle) and absolute anomaly of the extinction coefficient (bottom). The result obtained with exact Mie calculations are shown in red, while the approximation by the Ångström exponent is depicted by blue. Differences between the results obtained using the Ångström exponent conversion and Mie calculations are shown in the right panels.

First, we analyze the error associated with the conversion of SAGE II measurements to the wavelength of 750 nm. The aerosol extinction coefficients retrieved from SAGE II at 525 and 1020 nm are used to calculate the Ångström exponent, which is used then to convert the data to 750 nm. The results are presented in Figure 6. It is seen from the plot that the error associated with the conversion ranges from -7.25 to 9% and does not show any pronounced seasonal structure. For relative anomalies, the error is substantially reduced and is about 1%. The error for the absolute anomaly is within 9%, similar to that for the extinction coefficient.

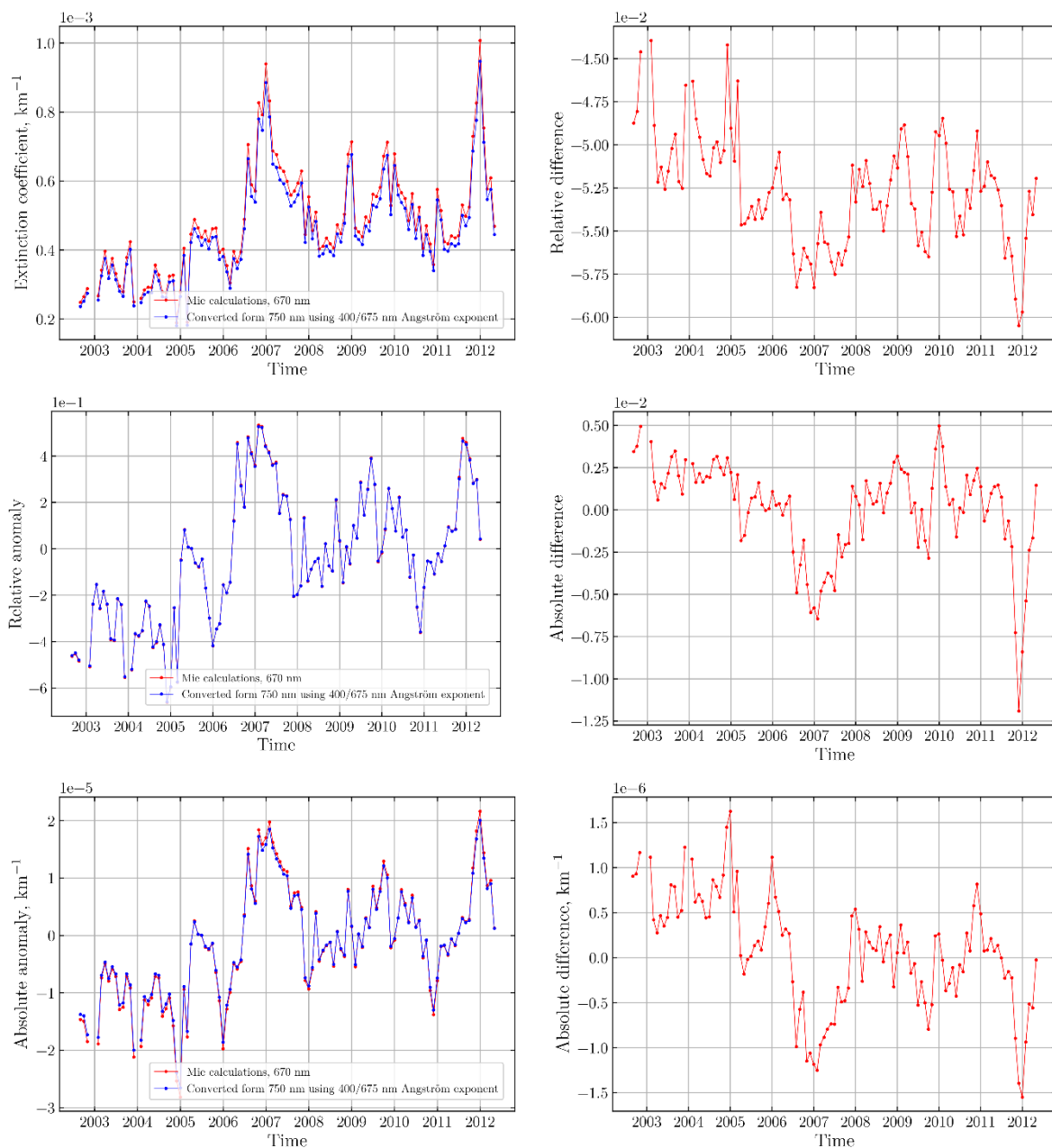


Figure 7. Error associated with the conversion of the aerosol extinction coefficient from SCIAMACHY (at 750 nm) to 670 nm using the Ångström exponent calculated from the GOMOS data at wavelengths of 400 and 670 nm. The left panels show the aerosol extinction coefficient (top), relative anomaly of the extinction coefficient (bottom) and absolute anomaly of the extinction coefficient (bottom). The result obtained with exact Mie calculations are shown in red, while the approximation by the Ångström exponent is depicted by blue. Differences

between the results obtained using the Ångström exponent conversion and Mie calculations are shown in the right panels.

Similar exercise was performed for the conversion of the SAGE II data to 670 and 870 nm wavelengths. As the spectral structure of the differences remains the same as for 750 nm, we do not show these plots here. The error for the extinction coefficient slightly decreases to 6.75 – 8.25% for 670 nm and 5.7 – 7.0% for 870 nm. At 670 nm the differences for the relative and absolute anomalies remain the same as for 750 nm while at 870 they decrease slightly to 0.9% and 7%, respectively.

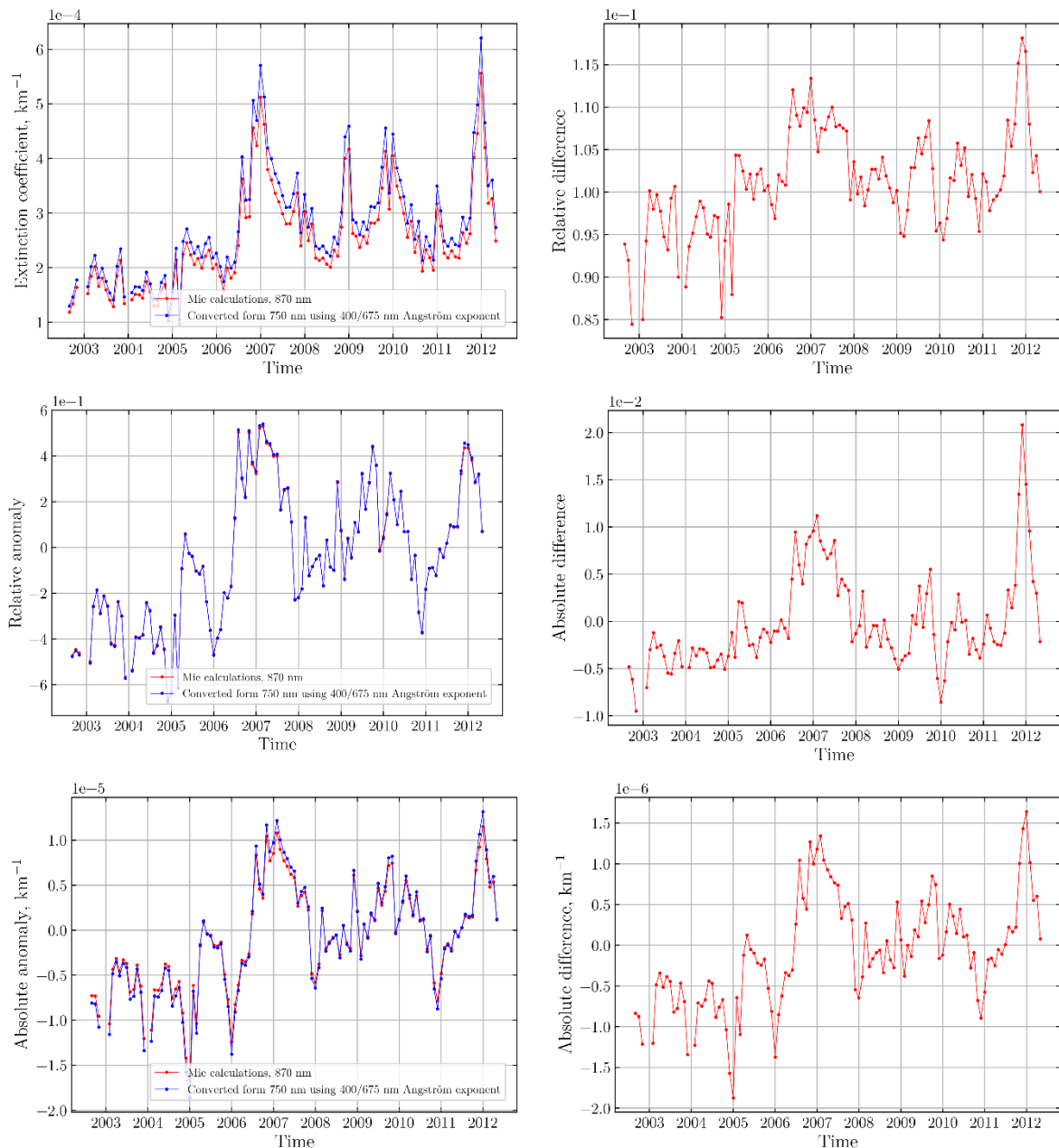


Figure 8. Same as Figure 7 but for 870 nm.

After the end of SAGE II mission in 2005 another source of information for the wavelength conversion needs to be found. One option is the usage of the aerosol extinction coefficients retrieved from GOMOS lunar occultation measurements at 400 and 670 nm to create a

climatology of Ångström exponents and use them then for the wavelength conversion. The errors associated with the conversion of SCIAMACHY data from 750 nm to 670 nm using the Ångström exponents calculated at GOMOS wavelengths are illustrated in Figure 7. It is seen that the error for the extinction coefficient ranges from 4.3 to 6.1% showing some seasonal structure. The error for the relative difference is about 1% and that for the absolute difference is about 6%.

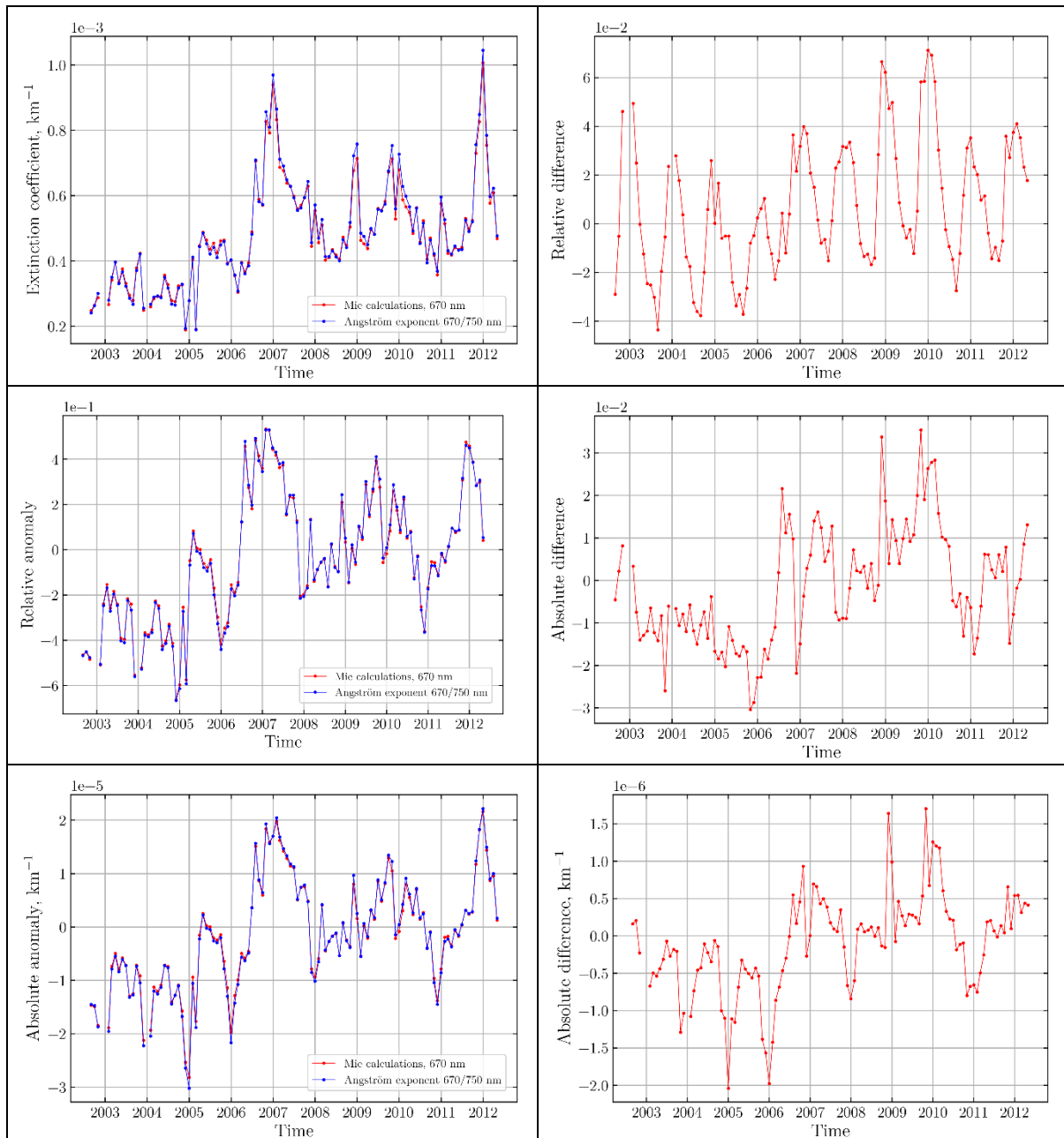


Figure 9. Error associated with the conversion of the extinction coefficient from 750 nm to 670 nm assuming a fixed particle size distribution. The left panels show the aerosol extinction coefficient (top), relative anomaly of the extinction coefficient (bottom) and absolute anomaly of the extinction coefficient (bottom). The result obtained with exact Mie calculations are shown in red, while the approximation by the Ångström exponent is depicted by blue. Differences between the results obtained using the Ångström exponent conversion and Mie calculations are shown in the right panels.

Figure 8 shows similar results but for the conversion to 870 nm. It is seen that the conversion error for the extinction coefficient increases and ranges now between 8.75 and 11.2%. Similarly, the error for the relative and absolute anomalies increases to 2 and 11%, respectively.

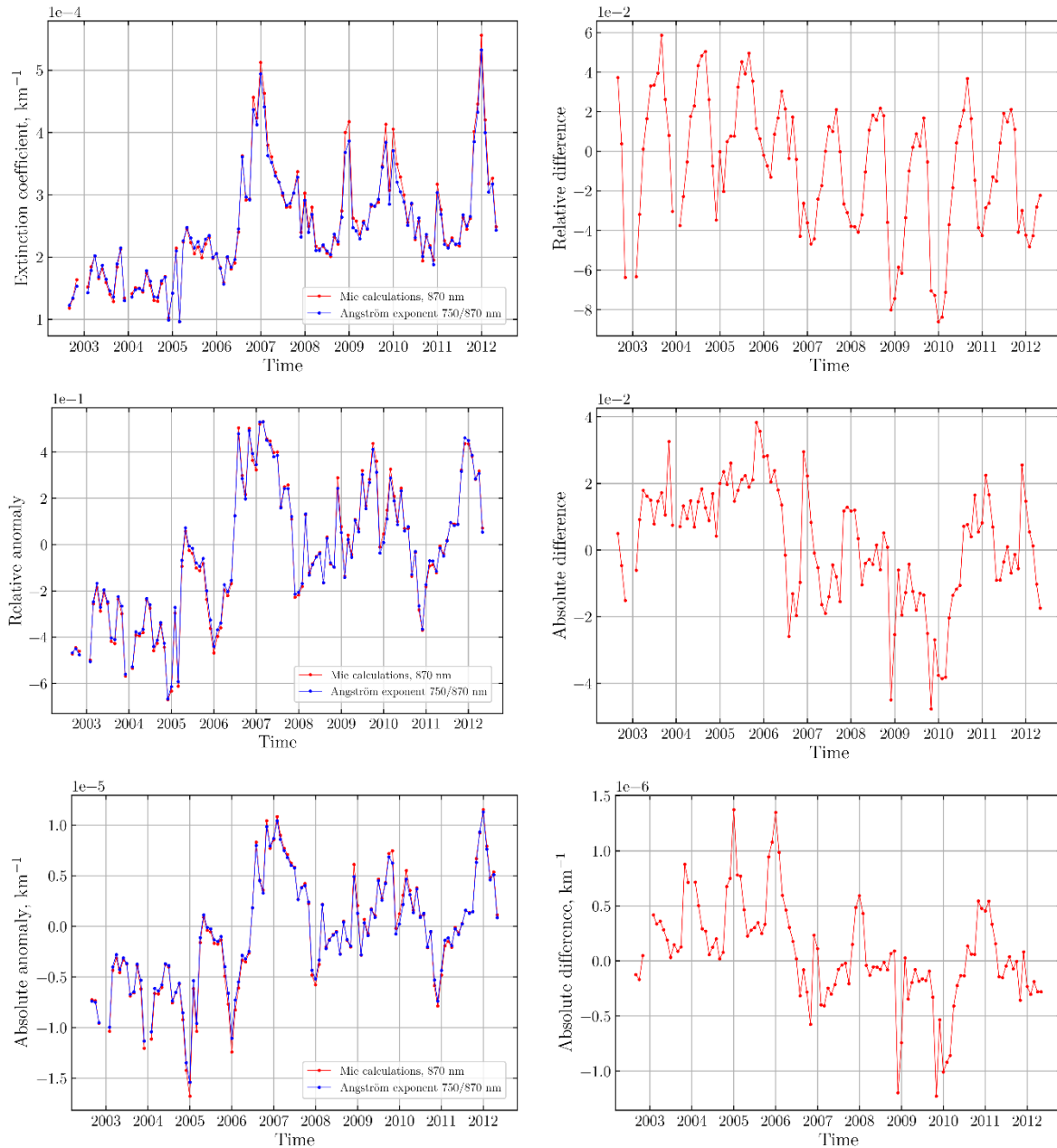


Figure 10. same as Figure 9 but for 870 nm.

For a comparison, we present the results of the conversion from 750 nm to 670 nm and to 870 nm assuming a fixed PSD in Figure 9 and Figure 10, respectively. For the extinction coefficient, the error ranges from -4 to 8% at 670 nm and from -8 to 6% at 870 nm. At both wavelengths, pronounced seasonal variations are seen. In comparison to the GOMOS Ångström exponent conversion, the maximum error associated with the fixed PSD assumption is similar at 670 nm and smaller at 870 nm, although the range of the error variation is much larger for both wavelengths. For the relative anomaly, the error is 5% for

670 nm and 6% for 870 nm, which is much larger than for GOMOS conversion. For the absolute anomalies, the errors are 6 and 8% for 670 and 870 nm, respectively, which is comparable with 6 and 11% from GOMOS conversion.

Main conclusions from the conversion error investigations are (i) the error is always smallest for the relative anomalies; (ii) conversion assuming a fixed aerosol PSD is associated with an error of 5-6% even then converting between the wavelengths, which are not far away from one another; and (iii) conversion using Ångström exponent calculated from measured data is usually associated with significantly smaller error for relative anomalies but might provide even worse results for the extinction coefficient time series. Based on these findings, the following way to create the climate record is proposed:

- Investigate if 670 or 870 nm is more favorable as the wavelength for the climate record
- Convert SAGE II to selected wavelengths using 525/1020 nm Ångström exponent
- For the selected wavelengths and merging approach, investigate if a conversion of SCIAMACHY and OSIRIS using 400/675 nm Ångström exponent from GOMOS is superior to that using the fixed PSD assumption

3.3 WP3. Improvement of the OMPS stratospheric aerosol extinction time series

Activities on the improvement of the OMPS stratospheric aerosol extinction time series consist of two major steps: identifying and fixing issues in the processing chain and optimizing the wavelength for the retrieval.

The optimization of the retrieval wavelength is especially crucial for OMPS because of its relatively coarse spectral resolution. To identify the optimal wavelength for the aerosol scattering coefficient retrieval from OMPS-LP data, the spectral ranges around the wavelengths of 670, 750 and 870 nm were investigated. To assess the implications for different types of the retrieval, both Sun-normalized radiance and the radiance normalized by the measurement at an upper tangent height (here 35 km) were considered. As a spectral bandwidth the range of $2 \times \text{FWHM}$ of the Gaussian spectral response function was assumed.

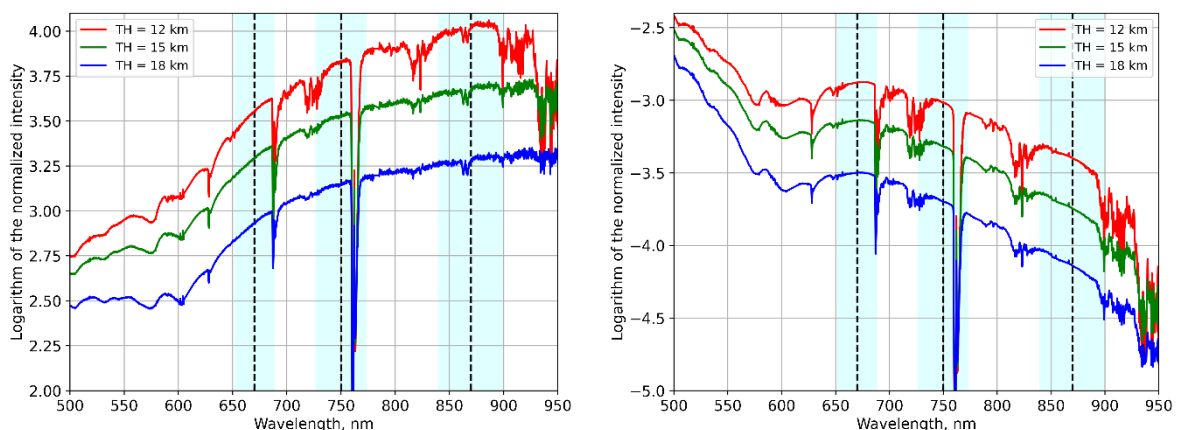


Figure 11. Limb-scatter radiance measured by SCIAMACHY at different tangent heights and OMPS-LP spectral bands. Left panel: radiance normalized to a limb measurement at 35 km tangent height. Right panel: Sun-normalized radiance.

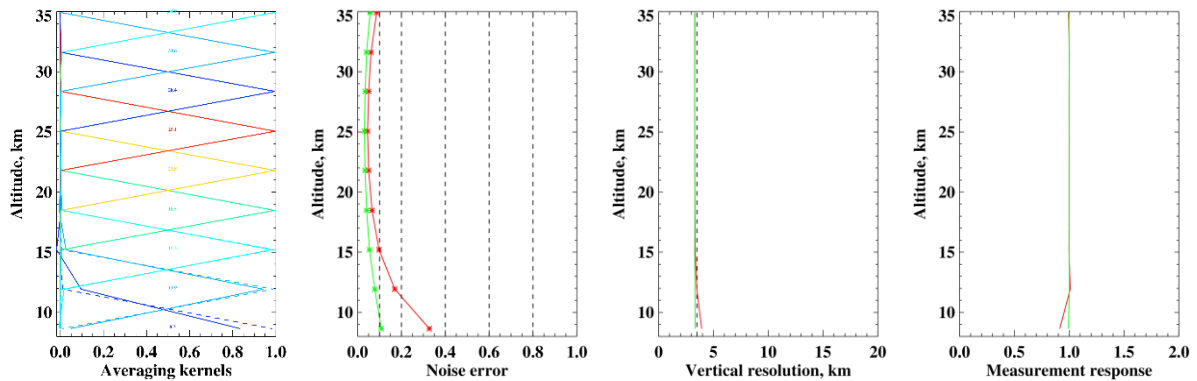


Figure 12. Retrieval characteristics (from left to right): averaging kernels (solid line for 670 nm, dashed line for 870 nm), retrieval noise error, vertical resolution and measurement response (red for 670 nm, green for 870 nm).

Figure 11 shows the limb-scatter radiances as measured by the SCIAMACHY instrument with the wavelengths of interest marked by the dashed lines and spectral bandwidths of the corresponding spectral pixels of OMPS-LP instrument marked by the green-blue color. Spectra for three different tangent heights are shown. The left panel shows the radiance normalized by the limb measurements at 35 km tangent height while the right panel shows the sun-normalized radiance. The following issues can be identified from the plots: (i) the spectral band centered at 670 nm touches the O₂ B absorption band (moderately strong) at its long wavelength boundary; (ii) O₂ A absorption band (extremely strong) is located in the middle of the spectral band centered at 750 nm; and (iii) the spectral band centered at 870 nm overlaps with H₂O absorption band (rather weak) at its long wavelength edge. Furthermore, then considering the measurements normalized to the upper tangent height, a weak spectral structure in the middle of the spectral band is observed, which might affect the retrieval. The obtained results show that the wavelength of 750 nm is least favorable. The band centered at 670 nm seems to be a preferable solution, although 870 nm can also be considered. It also seems reasonable to move both bands slightly towards shorter wavelengths. The centers at 655 nm and 865 nm are recommended as a result of the spectral data analysis.

To complete the investigation, the characteristics of the retrieval are compared for the wavelengths of 670 and 870 nm. Figure 12 shows retrieval characteristics for a selected tropical measurement, which are considered to be representative for all tropical observations. The averaging kernels shown in the left panel are quite similar for both wavelengths. Only at 8 km altitude, the averaging kernel for the 870 nm retrieval (dashed line) shows a somewhat larger peak value in comparison to that for 670 nm (solid line). The noise error, shown in the second panel from the left, is smaller for 870 nm (green line) than for 670 nm (red line) throughout the whole altitude range with differences increasing towards the low altitudes. The vertical resolution is quite similar for both wavelengths with the resolution at 670 nm being somewhat coarser at 8 km. A similar behavior is observed for the measurement response. In general, one can conclude that there is not much difference between the theoretical retrieval results at 670 and 870 nm.

One of the issues identified in the OMPS retrievals is a pronounced jump at the reference altitude indicating that the a priori aerosol number density profile used in the retrieval is too large at the reference altitude and above, see Figure 13. As the surface albedo is estimated using the measurement at the reference tangent height, the retrieval consequently pushes the estimated effective albedo to negative values. A trivial solution to decrease the a priori profile at the reference altitude and above might formally hide the issue forcing the retrieval to produce positive values for albedo but will still produce wrong results if the upper part of the profile is far from the reality. Thus, to increase the quality of the retrieved profiles an appropriate procedure to adjust the a priori profile at the reference tangent height and above is desired.

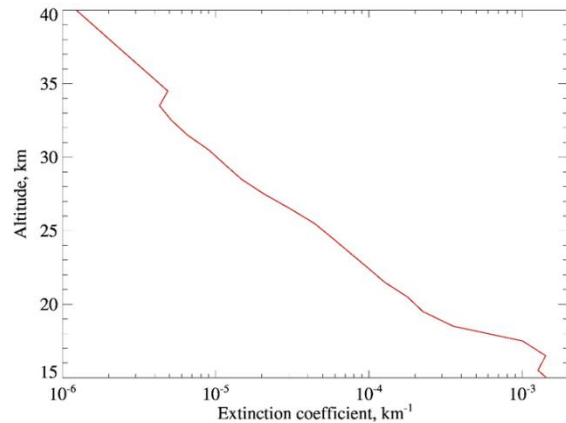


Figure 13. Example of the retrieved vertical profile of the stratospheric aerosol extinction coefficient

A possible solution we investigated in this work package is to allow the retrieval to scale the aerosol extinction coefficient following the solution at the uppermost retrieved altitude (typically one layer below the reference tangent height). To assess the adjusted algorithm all available data from 7 June 2017 until 31 August 2019 were retrieved and compared with the SAGE III/IIS data in the same way as done by (Malinina et al., 2021) for the standard retrieval version.

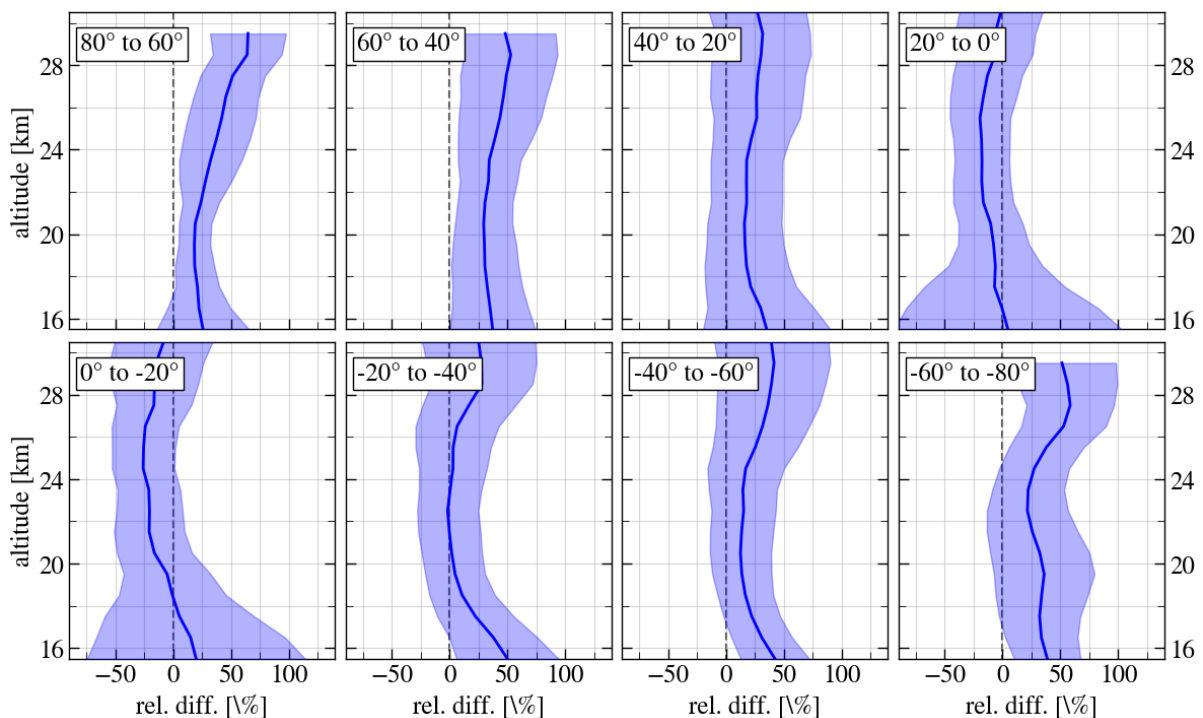


Figure 14. Comparison with SAGE III/IIS data for the standard retrieval version, V1.0.9 (published in (Malinina et al., 2021))

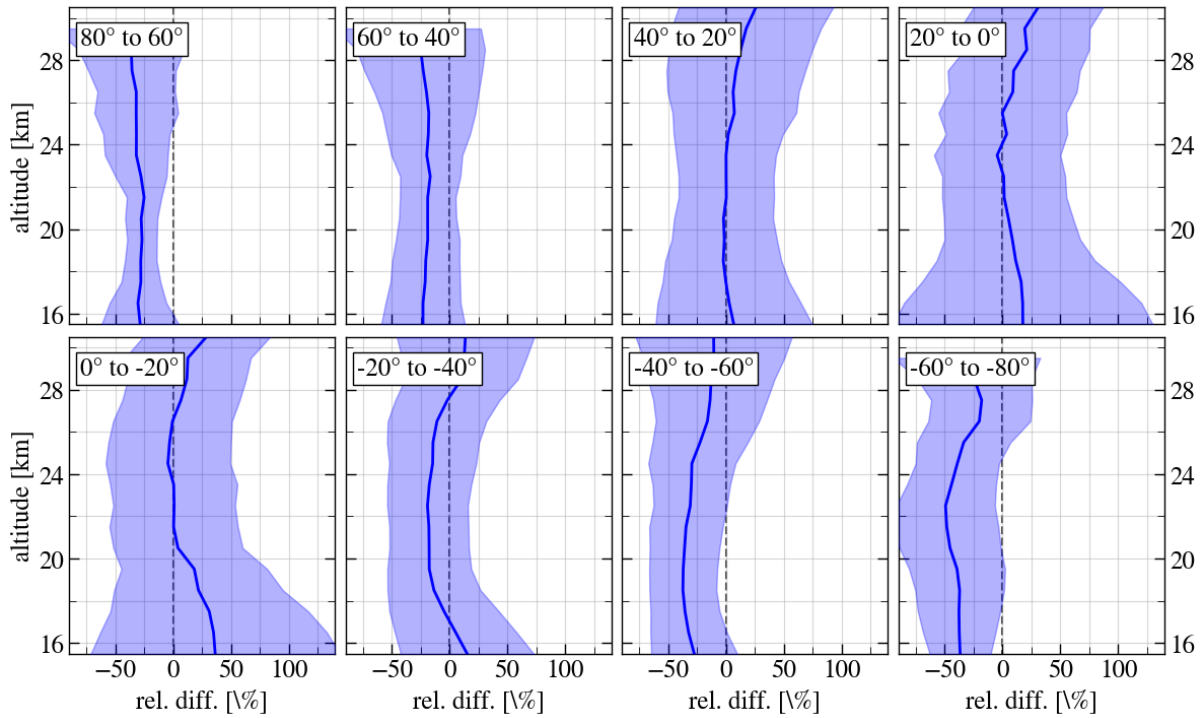
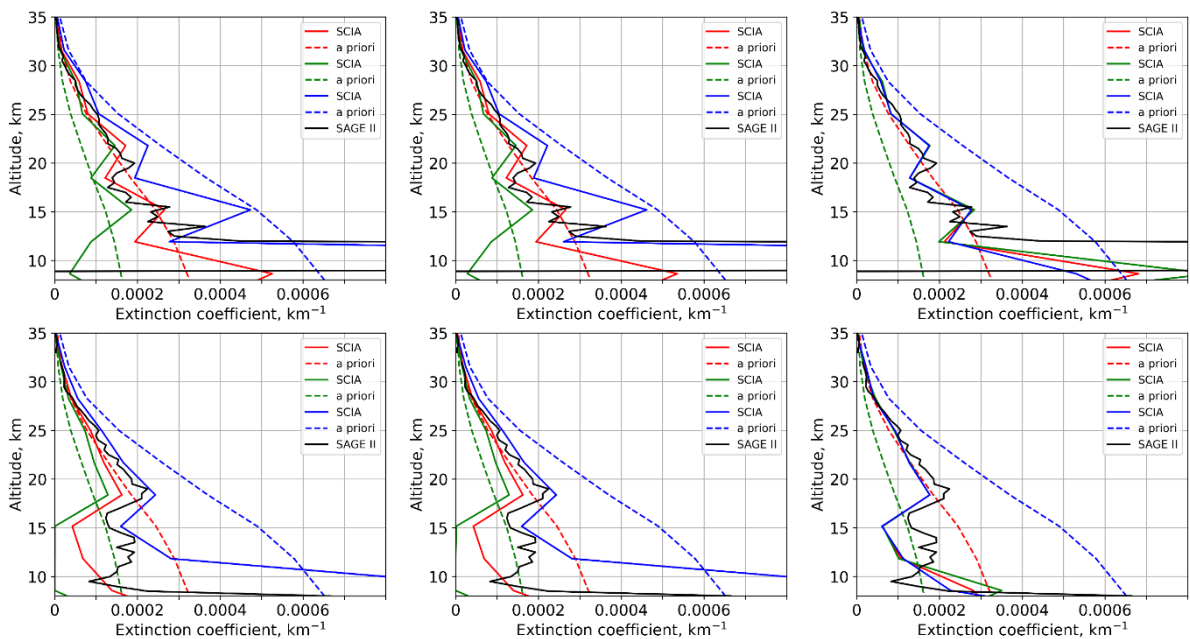


Figure 15. Comparison with SAGE III/ISS data for the updated retrieval version, V1.1

The comparison results for the standard retrieval version, V1.0.9, and for the updated retrieval version, V1.1, are shown in Figure 14 and Figure 15, respectively. It is seen from the plot, that the agreement becomes better between 20°S and 40°N while for other altitudes the difference just shifts towards negative values with maximum absolute difference values remaining nearly the same, i.e., in many cases an overcorrection is observed. Furthermore, the updated retrieval was found to be less stable tending under certain conditions to blow up the whole profile to unphysical values.



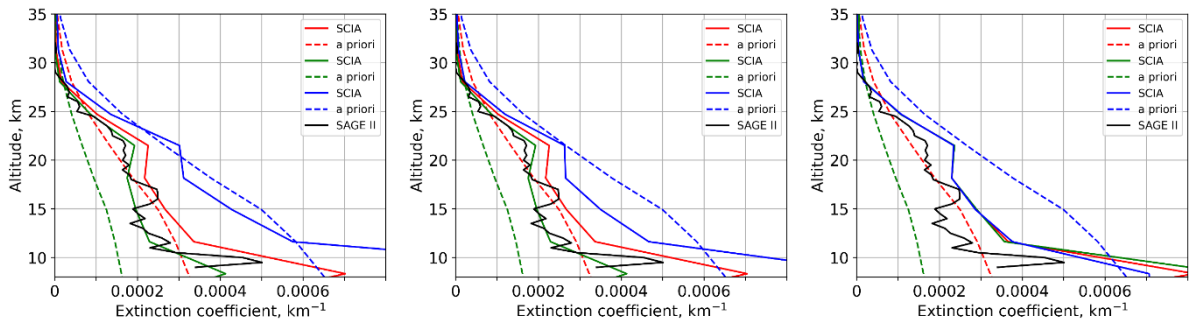


Figure 16: Dependence of the retrieved aerosol extinction profiles on the a priori information for different example measurements (shown in different rows). Left panels: results from the standard retrieval (normalization to the limb measurement at an upper tangent height around 38 km, albedo retrieval from the limb measurement at the reference tangent height). Middle panels: Aerosol retrievals using the sun-normalized radiance and albedo retrievals from the limb measurement at about 38 km tangent height. Right panels: Aerosol retrievals using sun-normalized radiance and albedo retrievals from the collocated nadir measurements.

A further attempt to reduce the influence of the aerosol extinction at the reference tangent height was made by using the normalization by the solar irradiance instead of the limb measurement at an upper tangent height. It is known, however, that a good knowledge of the surface albedo is more crucial for this approach. An attempt to use the same approach for the surface albedo retrieval as before, i.e., to retrieve it from the limb measurements at a tangent height around 38 km, showed that the resulting albedo strongly depends on the a priori aerosol extinction assumed around this altitude. Thus, another approach to constrain the surface albedo was required to increase the quality of the retrieval. At this point we switched to SCIAMACHY data and investigated the idea of exploiting the surface albedo information obtained from the collocated nadir measurements. This was not directly possible for the OMPS instrument because of a shorter spectral range of the nadir instrument (OMPS-NM) with the maximum wavelength of around 380 nm. The approach to collocate the SCIAMACHY limb and nadir measurements, retrieve the effective Lambertian surface albedo from SCIAMACHY nadir measurements and feed the retrieved values to the limb aerosol retrieval has been developed within the project. Example tests using different a priori information showed that the new retrieval is almost independent from the a priori aerosol extinction profile used in the retrieval. The results are illustrated in Figure 16 for three example measurements (shown in different rows). In all plots, different a priori aerosol extinction profiles used for the retrieval are shown by dashed lines and the resulting profiles of the aerosol extinction coefficients are depicted by the solid lines of the corresponding colors. For a comparison, results from collocated measurements from the SAGE II instrument are shown by the black solid line. In the left panels, results from the standard retrieval are shown. This retrieval employs the normalization to the limb measurement at an upper tangent height around 38 km and the effective Lambertian surface albedo is retrieved from the sun-normalized limb measurement at the reference tangent height. It is seen that the retrieval results strongly depend on the a priori aerosol extinction profile used for the retrieval. In the middle panels, results from a modified retrieval approach are shown, which uses the sun-normalized radiance to retrieve the aerosol extinction coefficient while the effective Lambertian surface albedo is still retrieved from the sun-normalized limb measurement at about 38 km tangent height. The plots reveal that there is no significant

change in the dependence on the a priori information as compared to the standard retrieval. This is explained by the fact that the retrieved surface albedo is influenced by the assumed aerosol extinction around 38 km. In turn, the retrieved aerosol extinction coefficients are strongly dependent on the retrieved surface albedo. In the right panels, the results of the new retrieval approach are shown, which employs the sun-normalized radiance to retrieve the aerosol extinction coefficient and uses the information on the effective Lambertian surface albedo retrieved from the collocated nadir measurements. It is seen that the dependence on the a priori aerosol extinction profile becomes insignificant down to about 12 km and is strongly reduced below.

The quality of the new SCIAMACHY aerosol extinction coefficient retrieval, which will be referred to as V3.0, was evaluated by a comparison with collocated SAGE II measurements for the year 2004. The results of this comparison for different latitude bands are presented in Figure 17. It is seen from the plot, that in the most latitude bands the results from the standard and new retrieval versions do not differ much down to 12 km. As the retrieval range in V3.0 was extended down to 8 km in comparison to 12 km in the standard retrieval (V1.4), larger differences at 12 km and below are expected. Contrary to other latitude bands, large differences between the results from the standard and new retrieval versions are found at southern mid-latitudes (20°S-60°S). Here, the differences change from about -50% to above +50%. As the measurements at southern mid-latitudes are made at scattering angles of 120-140 degrees, they are characterized by lower scattering signals and, hence, lower signal-to-noise ratios as compared to other latitude ranges. Therefore the retrieval in this latitude band is most challenging. The obtained results show that further optimization with respect to the albedo information used in the southern mid-latitudes is necessary. Because of a lack of resources, this work is outside the scope of the ESA-CREST project and is to be continued within a successor project.

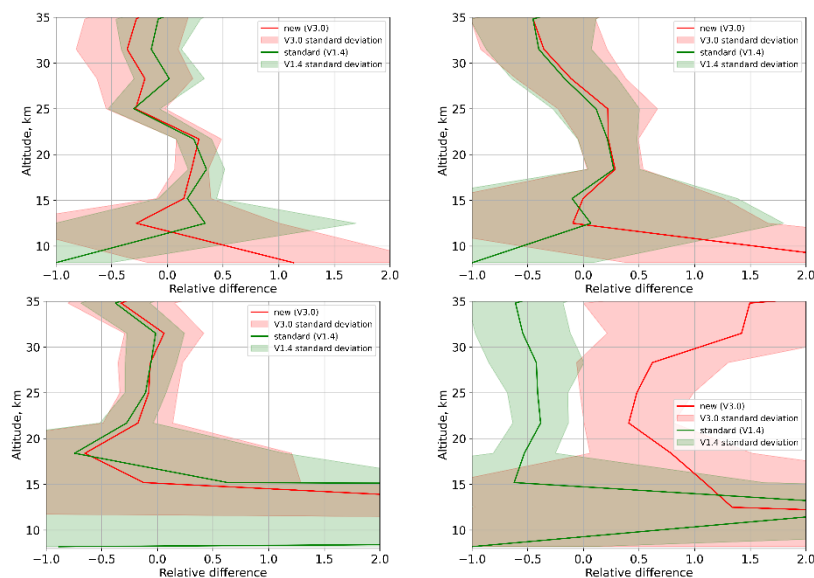


Figure 17: Comparison of the standard (V1.4) and new (V3.0) versions of the SCIAMACHY aerosol extinction coefficient retrieval with collocated SAGE II measurements for the year 2004 for different latitude bands. Top left: 60°N-90°N, top right: 20°N-60°N, bottom left: 20°N-20°S, bottom right: 20°S-60°S.

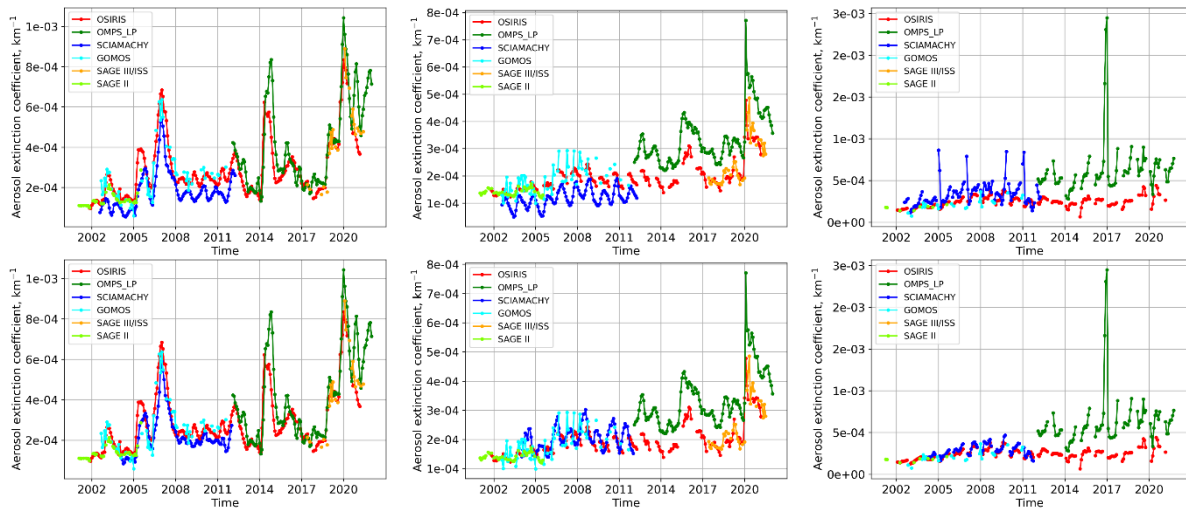


Figure 18: Comparison of the aerosol extinction coefficients from different instruments for the standard (top row) and new (bottom row) retrieval versions. The example comparisons are shown for the tropics, 5°N , at 21 km (left panels), southern mid-latitudes, 35°S , at 21 km (middle panels), and northern high latitudes, 75°N , at 18 km (right panels).

For a further assessment, the complete time series from the standard and new retrievals were compared to the results from other instruments (SAGE II, OSIRIS, GOMOS). Some example results of this comparison are shown in Figure 18. The results for the standard retrieval are shown in the top row while the bottom row shows the results from the new retrieval. The data from other instruments are the same in both plots. The left panels of the plot show the results for tropics (5°N) at 21 km. It is seen that the new retrieval results are systematically closer to the data from other instruments and do not show an unrealistically high annual variation any more, as seen e.g. between 2008 and 2012. For the southern mid-latitudes (35°S) at 21 km, as shown in the middle panels of the plot, the results from the new retrieval are also closer to the data from other instruments, although somewhat higher, and show more consistent seasonal variations. A similar behavior is observed for the high northern latitudes (75°N) at 18 km, as shown in the right panels of the plot. The new SCIAMACHY data are much closer to those from OSIRIS and GOMOS, show more consistent annual and inter-annual variations and the outliers present in the standard retrieval are removed.

In the other latitude bands and at over altitudes the agreement in terms of time series was found either to improve for the new data set or to remain at a similar level as for the old data. Thus, despite a larger bias in the southern mid-latitudes the SCIAMACHY V3.0 aerosol extinction coefficient data are rated as more suitable for creating a long-term multi-instrument time series.

Based on the outcome of the investigations with respect to the SCIAMACHY retrieval, a development of an improved algorithm to retrieve the aerosol extinction coefficients from OMPS-LP measurements has been started. As mentioned above, the spectral range of OMPS-NM instrument, which is capable of providing collocated nadir measurements, does not cover the aerosol retrieval wavelengths (longest available wavelength is 380 nm). Several attempts were made to match the albedo retrieved from limb and nadir measurements at 370 nm by adjusting the aerosol content at upper altitudes, but these attempts failed because of an inconsistency between the limb and nadir data. It was found that in most cases the surface

albedo retrieved from OMPS-NM measurements is higher than the limb albedo retrieved for an aerosol-free atmosphere. So, there was no obvious way to reach the nadir albedo in limb retrievals. Possible reasons for this behavior are currently under investigation.

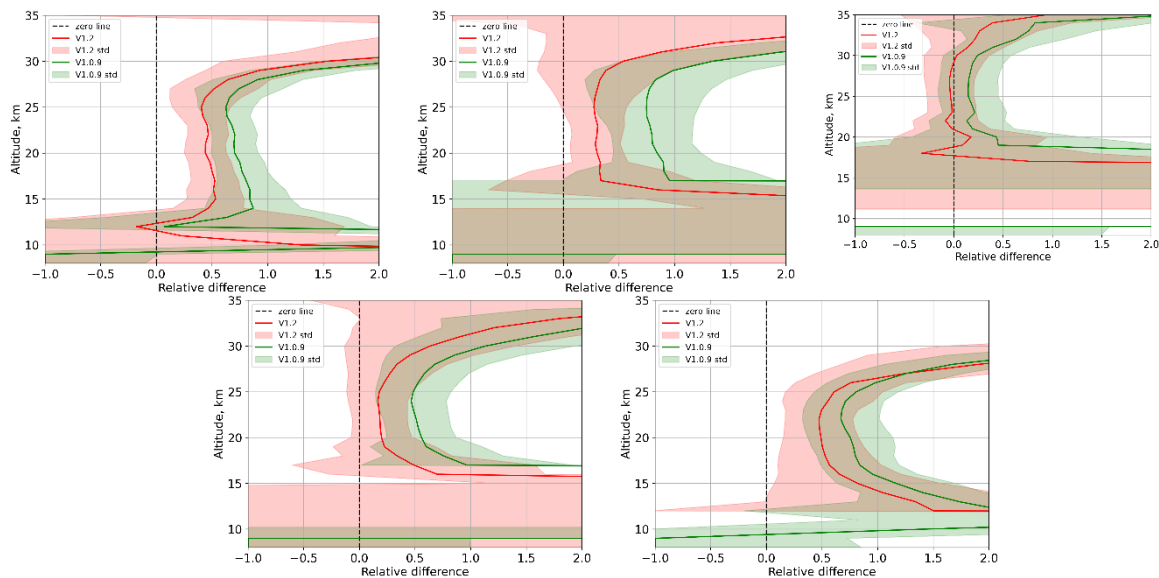


Figure 19: Comparison of the standard (V1.0.9) and new (V1.2) versions of the OMPS-LP aerosol extinction coefficient retrieval with collocated SAGE III/ISS measurements for the year 2018 for different latitude bands. Top left: 60°N-90°N, top middle: 20°N-60°N, top right: 20°N-20°S, bottom left: 20°S-60°S, bottom right: 60°S-90°S.

As a workaround, the basic principles of the standard retrieval algorithm were kept (normalization to the limb measurement at a reference tangent height and retrieval of the surface albedo from the sun-normalized radiance at the reference tangent height) but the selection of the reference tangent height was optimized by adopting the methodology used for OSIRIS retrievals (Bourassa et al., 2012). To determine the altitude range where the influence of the stratospheric aerosols and of the stray light is at minimum, the ratio of the measured radiance to the modelled Rayleigh radiance was calculated and the altitude where this ratio reaches the minimum was used as the reference tangent height. In the course of investigations, it was found that the non-linearity of the inverse problem is very high. Because of significant linearization errors, the retrieval does not stop at minimum fit residual but continues iterations making the results worse (in terms of fit residuals). To avoid this behavior, the improved algorithm stops the iterative process at the minimum of the fit residual. Similar to SCIAMACHY retrievals the lowest altitude of the OMPS-LP retrieval was extended down to 8.5 km compared to 12.5 km in the standard retrieval.

The quality of the improved OMPS-LP aerosol extinction coefficient retrieval, which will be referred to as V1.2, was evaluated by a comparison with collocated SAGE III/ISS measurements for the year 2018. The results of this comparison for different latitude bands are presented in Figure 19. It is seen from the plot, that for V1.2 retrieval the differences to SAGE III/ISS measurements are significantly smaller for all latitude bands. However, systematic overestimation by 25-50% is still seen all latitude band with exception of tropics.

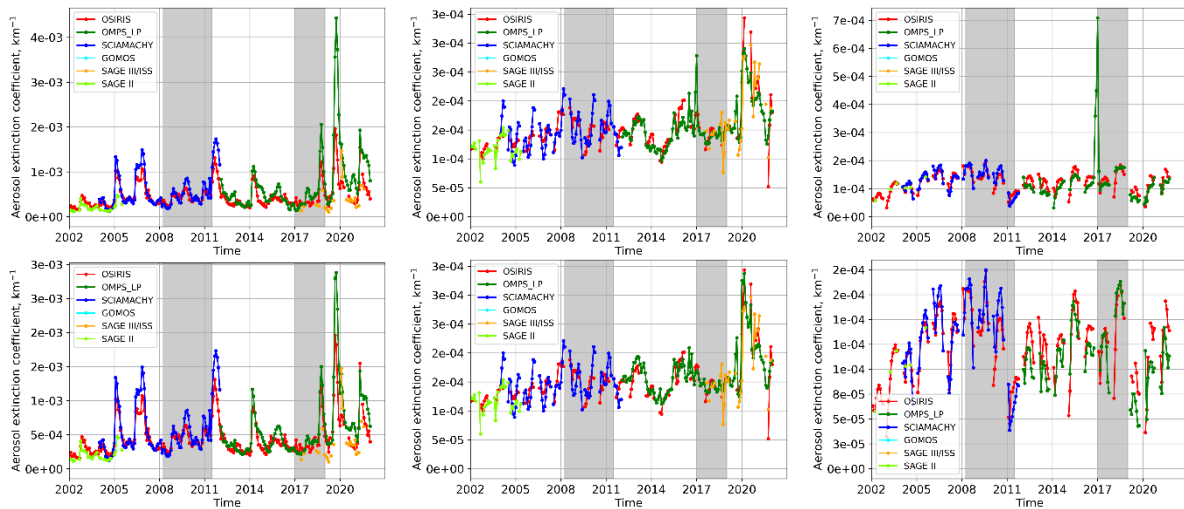


Figure 20: Comparison of the aerosol extinction coefficients from different instruments for the standard (top row) and improved (bottom row) retrieval versions. The example comparisons are shown for the tropics, 5°N , at 18 km (left panels), southern mid-latitudes, 55°S , at 18 km (middle panels), and northern high latitudes, 75°N , at 21 km (right panels). All data are scaled to OSIRIS measurements. The gray boxes depict ranges used for scaling.

For a further assessment, the complete time series from the standard and improved retrievals were compared to the results from other instruments (OSIRIS, SAGE III/ISS). Some example results of this comparison are shown in Figure 20. For clarity reasons, SCIAMACHY and OMPS-LP data are scaled to match OSIRIS time series. The results for the standard OMPS-LP retrieval are shown in the top row while the bottom row shows the results from the improved OMPS-LP retrieval. The data from other instruments are the same in both plots. The left panels of the plot show the results for tropics (5°N) at 18 km. It is seen that for the years after 2019 the agreement between OMPS-LP and OSIRIS data is much better for the improved retrieval version. For the southern mid-latitudes (55°S) at 18 km, as shown in the middle panels, some spikes at the end of 2016 and the beginning of 2017 are removed by the improved retrieval and a better agreement within the aerosol peak in the beginning of 2020 is observed. In the northern high latitudes (75°S) at 21 km, as shown in the right panels of the plot, the outliers in the end of 2016 and the beginning of 2017 are removed by the improved algorithm, making the agreement with OSIRIS data much better. In general, however, the scaled time series of the aerosol extinction coefficient from the improved algorithm are very similar to those from the standard retrieval.

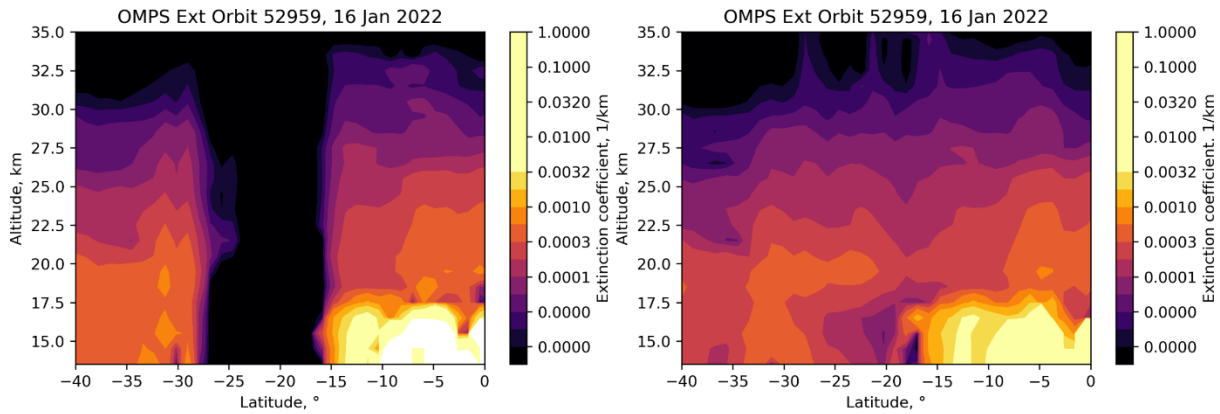


Figure 21: Aerosol extinction coefficient retrieved from OMPS-LP measurements after the eruption of the Hunga Tonga–Hunga Ha’apai volcano in the beginning of 2022 by using the standard (left panel) and the improved (right panel) algorithms.

A major drawback of the retrieval algorithms employing the normalization to the reference tangent height is a strong dependence of the results on the aerosol extinction assumed near the reference tangent height. In a rare case of high aerosol loading at very high altitudes, as it happened after the eruption of the Hunga Tonga–Hunga Ha’apai volcano in January 2022, the retrieval might drastically underestimate the aerosol extinction in the whole altitude range of the retrieval, as it is illustrated in the left panel of Figure 21. The optimization of the selection of the reference tangent height employed in the improved retrieval version, enable us to mitigate this issue, as illustrated in the right panel of Figure 21.

In conclusion, version 1.2 of the OMPS-LP retrieval algorithm newly developed within this project substantially reduces the bias in the retrieved aerosol extinction coefficients, mitigates the issue with a strong underestimation of the aerosol extinction in a case of a strong aerosol loading at very high altitudes, and removes outliers in the time series. However, an overall bias of 25-50% still persists in all latitude bands with the exception of tropics.

To reduce the remaining bias, additional investigations on the optimal retrieval setup were performed. Promising preliminary results were obtained when using the sun-normalized radiance, extending the retrieval range up to 50 km but setting the aerosol profile above 46 km to zero and retrieving the effective Lambertian surface albedo from all tangent heights between 8 and 50 km. This configuration implies that the tangent heights above 46 km are only used to retrieve the albedo, but the albedo retrieval is additionally stabilized by the measurements at lower tangent heights. A few retrieval examples for single measurements are shown in Figure 22. The upcoming retrieval version is denoted as V2.0. The plot reveals that the upcoming retrieval version V2.0 in most cases removes the bias seen in V1.2 and agrees very well with collocated SAGE III/ISS measurements. However, for some measurements, e.g., the right panel in the top row and the middle panel in the middle row, the aerosol extinction coefficient is underestimated. Investigations for an extended collocation data set are ongoing.

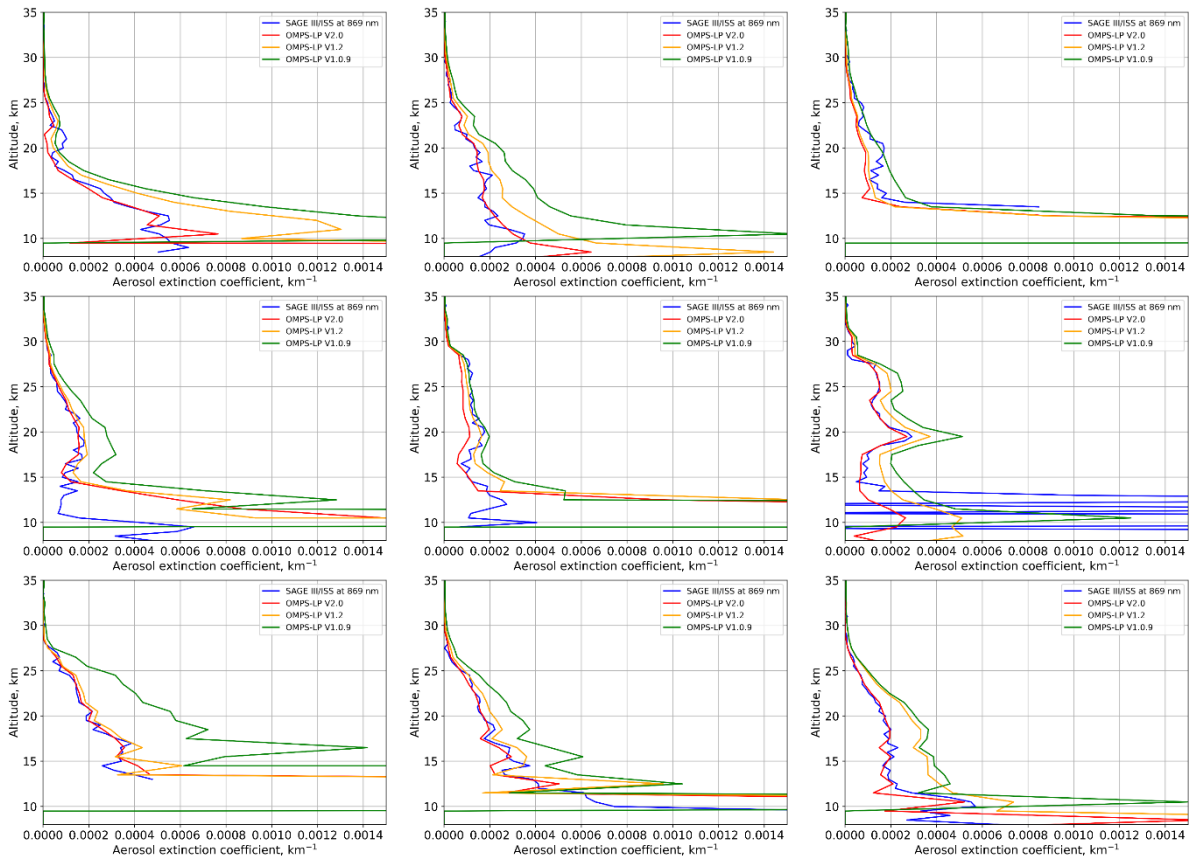


Figure 22: Example comparison of the standard (V1.0.9), improved (V1.2) and upcoming (V2.0) versions of the OMPS-LP retrieval with SAGE III/ISS measurements for single measurements. The measurements were performed at the following latitudes: 66°S (top left), 51°S (top middle), 45°S (top right), 30°S (middle left), 1°N (middle middle), 21°N (middle right), 39°N (bottom left), 59°N (bottom middle), 70°N (bottom right).

3.4 WP 4. New data set of aerosol extinction coefficient from GOMOS stellar occultation measurements

3.4.1 Introduction: motivation for the study

The GOMOS aerosol data are important for climate studies. They have been already used in the merged stratospheric aerosol datasets (Vernier et al., 2011) and climate studies (Solomon et al., 2011; Santer et al., 2014).

The aerosol extinction coefficient data record at 500 nm and the spectral dependence of aerosol extinction approximated by the 2nd order polynomial is available so from GOMOS star occultation measurements, for both the ESA IPF v.6.0 (Kyrölä et al., 2010) and AERGOM (Vanhellemont et al., 2016) processors. However, the reported spectral dependence of GOMOS aerosol extinction is often not realistic, mainly due to interference with ozone retrievals, limited wavelength range in the IPF v6 retrievals, insufficient signal-to-noise ratio, and limitation of the polynomial model. In particular, it is known that lower stratospheric ozone in IPF v6 has a strong bias, and this influences the quality of aerosol retrievals, as ozone and aerosols are retrieved simultaneously in both IPFv6 and AERGOM.

We aim to create multi-wavelength aerosol extinction profiles (climate data record) from averaged GOMOS transmittances. We follow the approach of (Sofieva et al., 2017a), which provides the realistic ozone values in the UTLS. The proposed new algorithm for aerosol retrievals is based on the removal of extinctions due to Rayleigh scattering and absorption by ozone and other trace gases from GOMOS transmission spectra.

3.4.2 The inversion algorithm

3.4.2.1 Preparation for retrievals: creating averaged transmittances dataset

The monthly averaged transmittances $T(\lambda, z)$, λ is a wavelength and z is a tangent altitude, are used as a starting point for the retrievals. The advantages of this approach are (i) better signal-to-noise ratio and (ii) residual scintillations are removed.

For computing averaged transmittances, we used GOMOS nighttime measurements (with solar zenith angle at the ray perigee point larger than 107°). Averaged transmittances for years 2002-2005 were processed in the ESA project ALGOM by BIRA. We processed the data from remaining years (2006-2011) at FMI. The methodology is the same as it was used in the ALGOM: it includes interpolation of transmittances at a fixed altitude grid, outlier filtering, and data averaging. The outlier filtering is performed using an algorithm based on the well-known Jack-knife method. The threshold for outliers has been chosen as 3 standard deviations from the median.

For each tangent altitude and each wavelength, the average transmittance is computed as the weighted median transmittance. This estimate is insensitive to outliers, and it takes into account the signal-to-noise ratio of different measurements, which can differ considerably for GOMOS. The transmittances are weighted with respect to the inverse of their estimated measurements errors.

A weighted median calculation starts by sorting the transmittance values in increasing order and rearranging the associated weights in the same fashion. The cumulative distribution of these weights is subsequently evaluated. The weighted median is then the transmittance value corresponding to the 50% level of this cumulative weight distribution.

The routines were optimized for numerical efficiency.

The examples of averaged transmittances for the latitude bin $0-10^\circ\text{N}$ are shown in Figure 23, for conditions of low aerosol level (January 2003, left panel of Figure 23) and increased aerosols after volcanic eruptions (January 2007, right panel). It is clearly seen that the transmittances are lower (optical depth is higher) for the volcanic aerosol conditions (compare transmittances at 20 km, thick red lines).

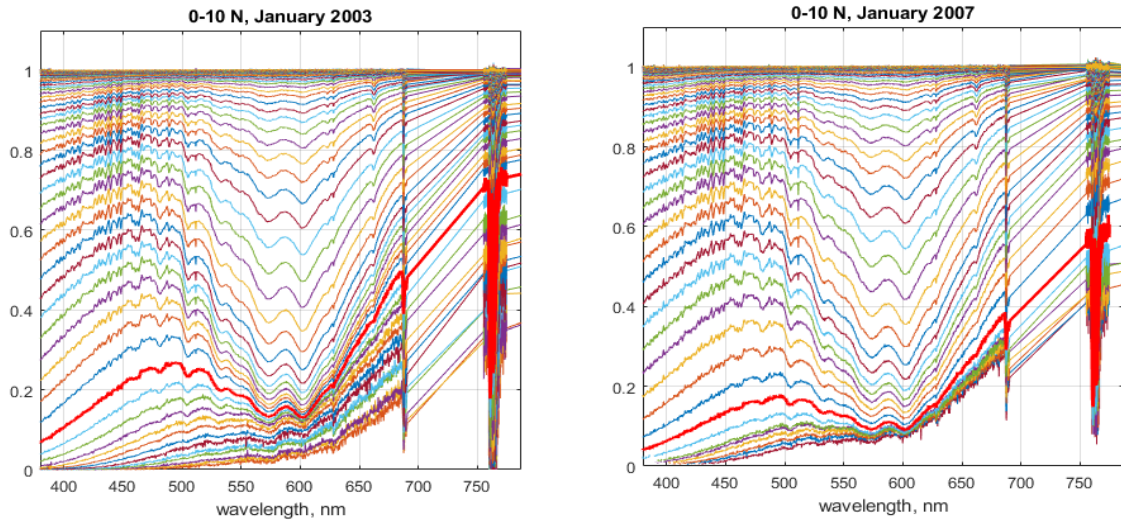


Figure 23. Examples of GOMOS averaged transmittance spectra in the equatorial region 0-10°N, in January 2003 (background aerosols) and in January 2007 (after volcanic eruptions). Red thick lines highlight transmittances at 20 km.

3.4.2.2 Aerosol retrieval algorithm

The idea of aerosol retrievals from averaged transmittances is very simple: the extinction due to Rayleigh scattering and due to absorption of ozone, NO₂ and NO₃ are removed from the GOMOS extinction spectra. The remaining part is due to aerosol extinction.

We used data from spectrometer A at wavelengths 380-672 nm and spectrometer B1 at wavelengths 755-759 nm. The NO₂ and NO₃ optical depth is computed using retrieved GOMOS NO₂ and NO₃ profiles. The Rayleigh extinction is computed using ECMWF air density data provided in the GOMOS files. As in ALGOM2S retrievals (Sofieva et al., 2017a), ozone optical depth is computed using a DOAS-type retrieval with the triplet in the Chappuis band (reference wavelengths: 523 – 527 nm, 673–677 nm and absorbing wavelengths: 598–602 nm). During our development, we used both cross-sections used in GOMOS retrievals and also Serdyuchenko cross-sections, but the result is nearly the same. In the processing, we filtered out unreliable transmittance values (with large uncertainties, >100 %).

The details of retrievals of horizontal aerosol optical depth are illustrated in Figure 24 for altitude 20 km near Equator (0°-10°S). The measured total optical depth, $\tau(\lambda, z) = -\log(T)$, is shown by the black line. The estimated optical depths due to ozone (τ_{ozone}), NO₂ (τ_{NO_2}), NO₃ (τ_{NO_3}) and Rayleigh extinction (τ_{air}) are shown by colored lines in the upper panel of Figure 24.

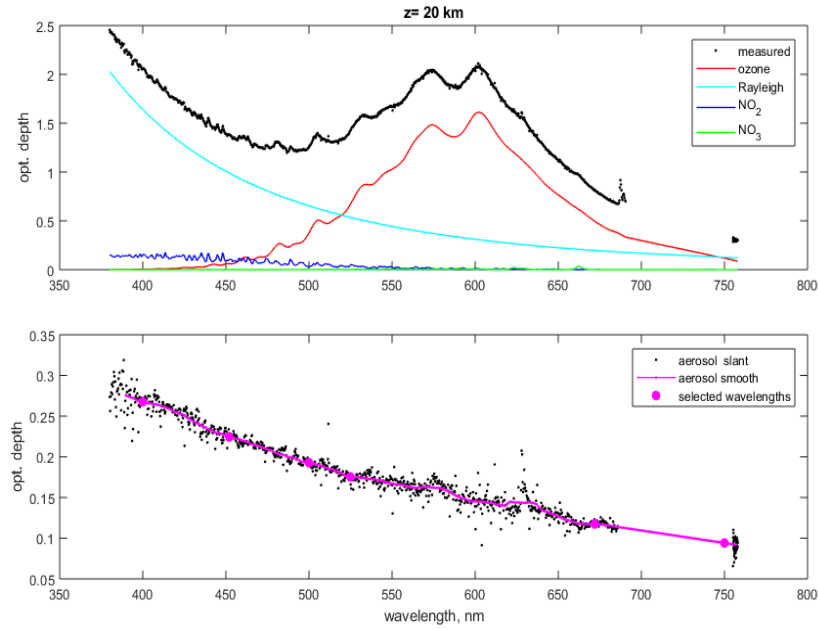


Figure 24. Illustration of GOMOS aerosol retrieval algorithm. Top: measured optical depth spectrum (black) and contributions due to ozone (red), Rayleigh scattering (cyan), NO_2 (blue) and NO_3 (green). Bottom: original (black) and smoothed (magenta) residuals.

The resulting residuals:

$$R(\lambda, z) = \tau(\lambda, z) - \tau_{\text{ozone}}(\lambda, z) - \tau_{\text{air}}(\lambda, z) - \tau_{\text{NO}_2}(\lambda, z) - \tau_{\text{NO}_3}(\lambda, z) \quad (1)$$

are due to aerosols. The residual profiles are smoothed and taken at 9 wavelengths: 400, 440, 452, 470, 500, 525, 550, 672 and 750 nm. The result of this spectral inversion is horizontal column aerosol optical depth profiles $\tau_{\text{aero}}(\lambda, z)$.

In the vertical inversion, the profiles of local extinction are reconstructed from the horizontal column aerosol optical depth profiles $\tau_{\text{aero}}(\lambda, z)$, for each wavelength.

The GOMOS vertical inversion is linear, and it is performed in the same way as in the GOMOS processor (Kyrölä et al., 2010). The target-resolution Tikhonov-type regularization is applied in the vertical inversion (Sofieva et al., 2004; Kyrölä et al., 2010). The resulting actual resolution of the aerosol profiles $\beta(\lambda, z)$ is 3 km.

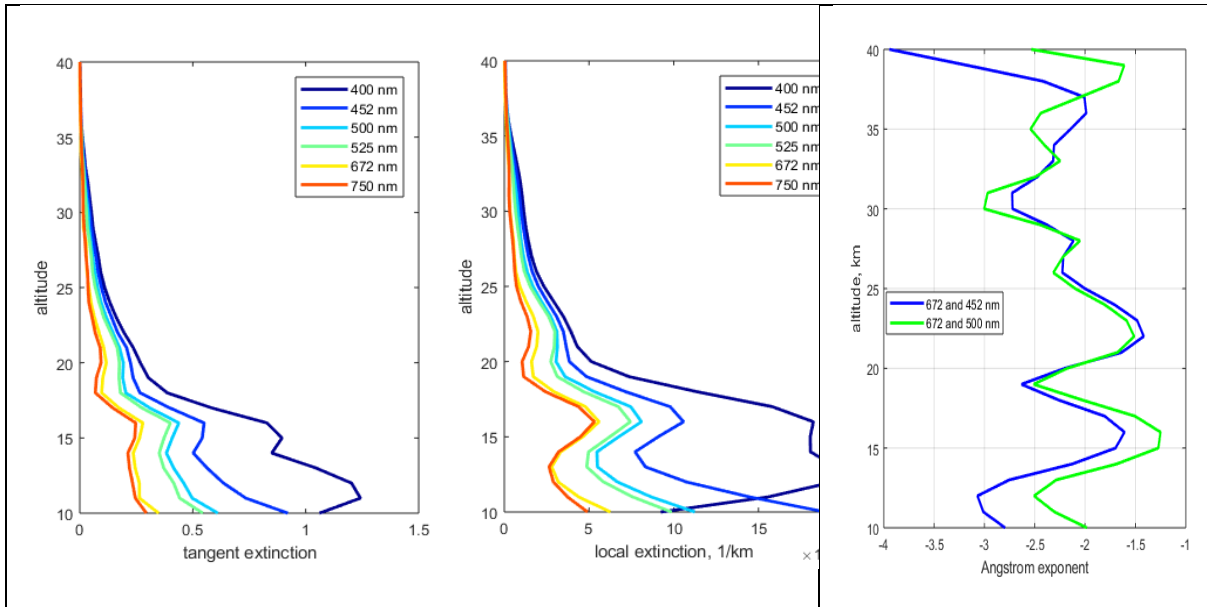


Figure 25. The retrieved horizontal column(left) and local (center) extinction profiles for September 2002, 10-20 S (wavelengths are indicated in the legend). Right: the Ångström exponent profiles estimated using different combinations of wavelengths

The examples of retrieved horizontal column and local aerosol extinction profiles are shown in Figure 25. One can notice the expected spectral dependence of aerosol extinction: it is larger for shorter wavelengths. The profiles of the Ångström exponent $\alpha = \frac{\log(\beta(\lambda)/\beta(\lambda_0))}{\log(\lambda/\lambda_0)}$ for different wavelength combinations are shown in the right panel of Figure 25. The values of the Ångström exponent are in the expected range, with an expected decrease with altitude.

3.4.3 Retrieval results and intercomparisons

The multi-wavelengths new GOMOS aerosol retrievals allow direct comparison of aerosol profiles from different instruments. Figure 26 shows the comparison of GOMOS and SAGE II aerosol profiles at 525 nm in September 2002. One can observe nearly perfect agreement with SAGE II above 20 km. Below 20 km GOMOS aerosol extinction is larger, but it is in a good agreement with SAGE II extinction with omitted cloud filtering (compare magenta and blue lines in Figure 26). Using averaged transmittances does not allow exclude cirrus clouds cases, which might result in overestimation of aerosol extinction below 20 km.

Figure 27 shows the GOMOS and SAGE II aerosol profiles at several wavelengths. The GOMOS and SAGE II spectral dependence of aerosol extinction profiles are similar above 20 km, but they differ below 20 km. Since the retrievals are performed using the average transmittances, the presence of clouds is not easy to detect: the monthly averaged spectral dependence of extinction is different from that of the local extinction in cloudy conditions, as expected.

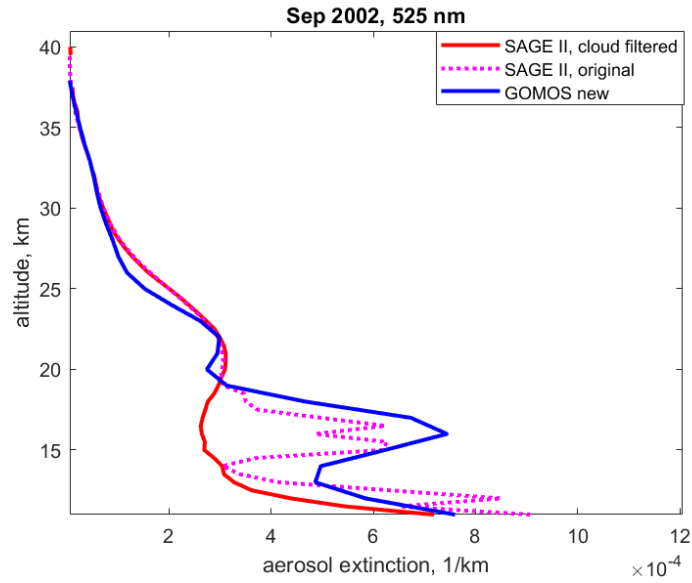


Figure 26. Comparison of GOMOS and SAGE II aerosol extinction profiles at 525 nm, September 2002, 10-20 S

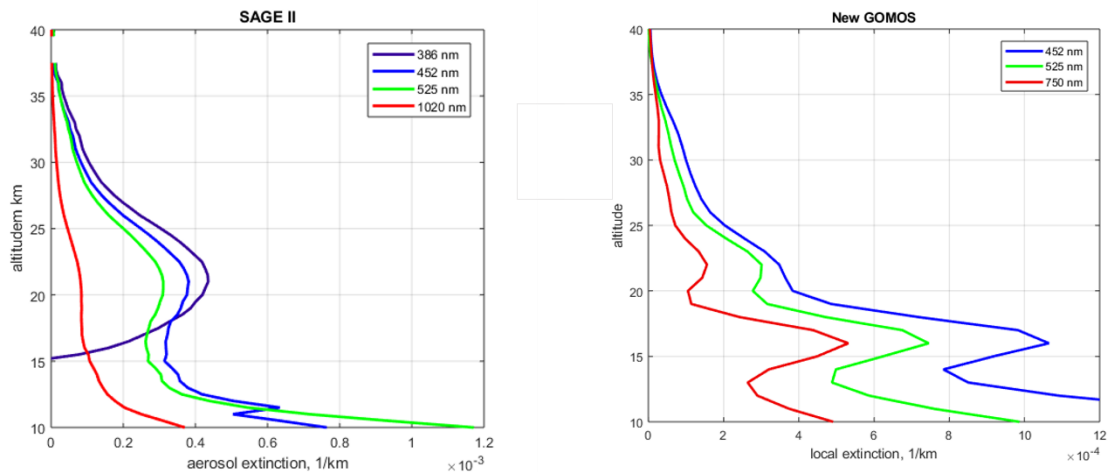


Figure 27 Comparison of GOMOS and SAGE II aerosol profiles at several wavelengths, September 2002, 10-20 S. The wavelengths are specified in the legend.

Figure 28 shows the monthly average new GOMOS and AERGOM aerosol extinction profiles in the same latitude band 10°-20° S, in September 2002. Above 20 km, the aerosol extinction profiles and their spectral dependence are similar. Below 20 km, the profiles are different: in our retrievals, aerosol extinction is larger for shorter wavelengths, while the opposite (unrealistic) behavior is observed in AERGOM data.

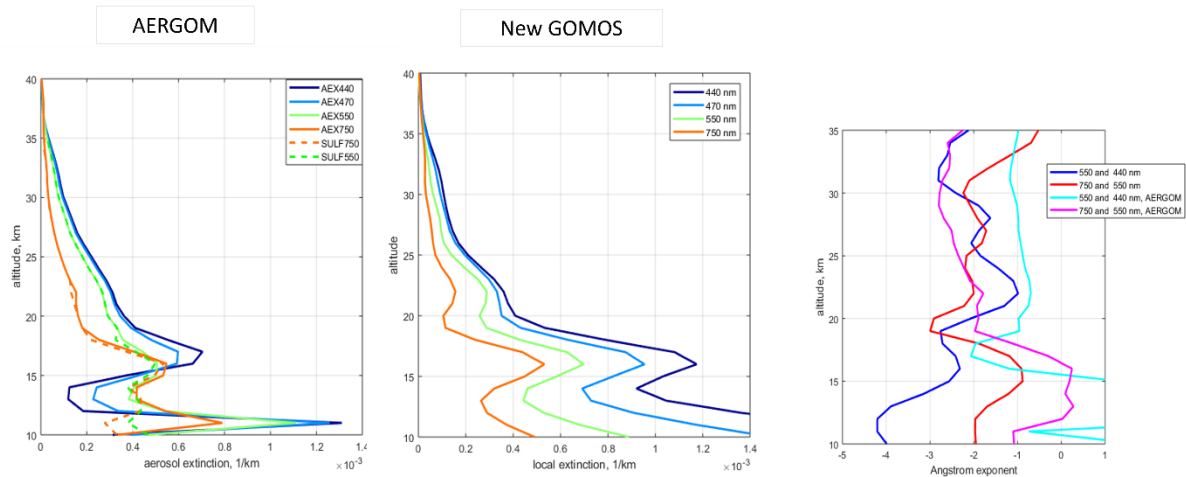


Figure 28. AERGOM (left) and new GOMOS (center) aerosol extinction profiles at several wavelengths. Right: profiles of the Ångström exponent. The data are for September 2002, 10°-20° S.

Figure 29 compares GOMOS profiles for September 2002 in the latitude zone 10°-20°S, with the averaged profiles from several satellite instruments. At 525 nm, our retrievals are compared with AERGOM at 550 nm, SAGE II, and SCIAMACHY measurements. At 750 nm, new GOMOS aerosol profile is compared with AERGOM, SCIAMACHY and OSIRIS data. In both comparisons, the SCIAMACHY data are from the special retrievals with the reconstruction of the particle size distribution. In general, GOMOS aerosol extinction profiles are very close to those of other instruments above 20 km. The best agreement is with SAGE II and OSIRIS data. At lower altitudes, the GOMOS aerosols are biased toward larger values in case of cirrus clouds presence. This feature is present in our retrievals and also in the AERGOM dataset.

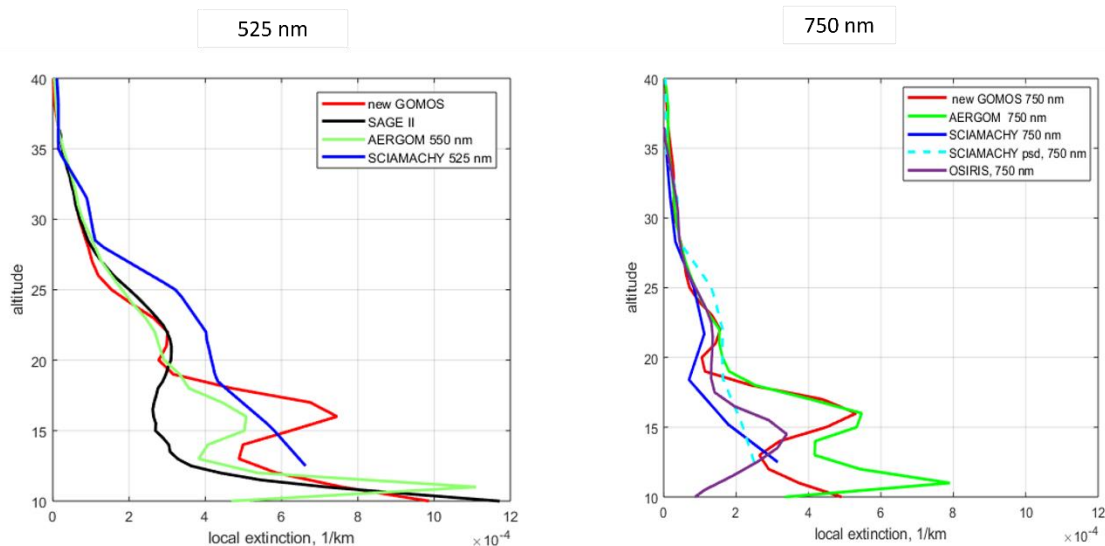


Figure 29. Comparison of new GOMOS retrieved profiles for September 2002, 10-20 S, with data from several satellite instruments. Left panel: comparisons for the wavelength 525 nm, right panel: comparisons for the wavelength 750 nm.

We tried to apply various methods for cloud filtering in averaging GOMOS transmittances—according to absolute values of extinction and ratio at different wavelengths. However, the

effect is rather minor. We also investigated another hypothesis - non-perfect refractive dilution correction due to imperfectness of ECMWF data (note that very old ECMWF forecast data have been used in the GOMOS processor). Although some improvement is observed when ERA-5 data are used, it does not completely remove the enhancements in the retrieved aerosol extinction near the tropical tropopause.

3.4.4 GOMOS aerosol climate data record

The whole GOMOS dataset has been processed. After processing, we filtered out the data points that have unrealistic values of Ångström exponent ($\alpha < -4$ below 27 km) or potentially affected by clouds ($\alpha > 0.2$).

We examined outliers in the processed GOMOS-FMI aerosol dataset and found that one of the reasons for strong outliers is insufficient amount of data used for averaged transmittances. Therefore, the data based on a small number of averaged transmittances are excluded from the final GOMOS aerosol dataset.

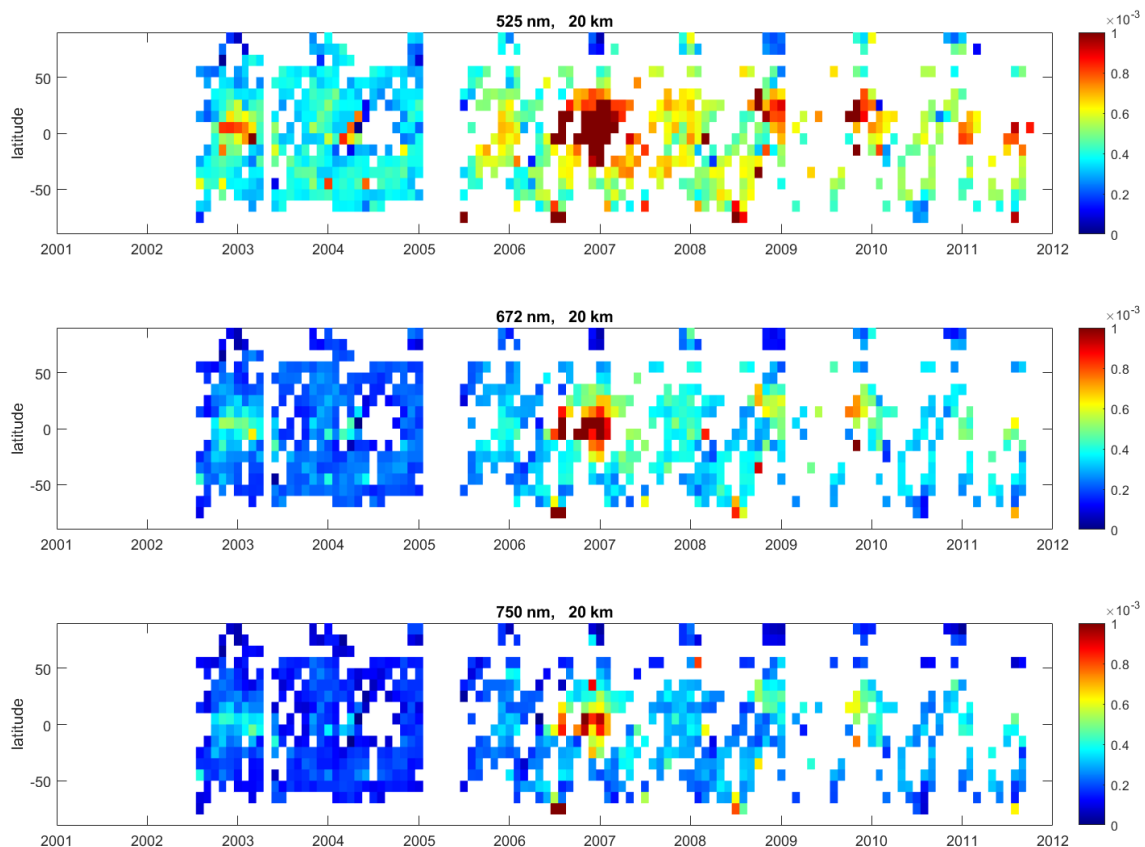


Figure 30. Time series of aerosol extinction(1/km) at 20 km for 525 nm (top), 672 nm(center) and 750 nm (bottom).

Figure 30 shows the time series of stratospheric aerosols at 20 km for 3 wavelengths 525nm, 672 nm and 750 nm. The volcanic eruption conditions in 2007, 2009 and 2010 are clearly seen in Figure 30. The time series for 672 nm and 750 nm look similar, which suggests that the aerosol extinction at 750 nm has a quality similar to that at 672 nm.

Figure 31 shows the time series of aerosol extinction at 20 km in the latitude zones 30°-50° S (top), 20°S-20°N (center) and 30°-50° N (bottom), for all retrieved wavelengths. The shapes of aerosol extinction spectra look according to the expectations. The enhancements due to volcanic eruptions - Soufrière Hills in May 2006, Kasatochi in August 2009 and Sarychev in June 2009 - are seen in the data.

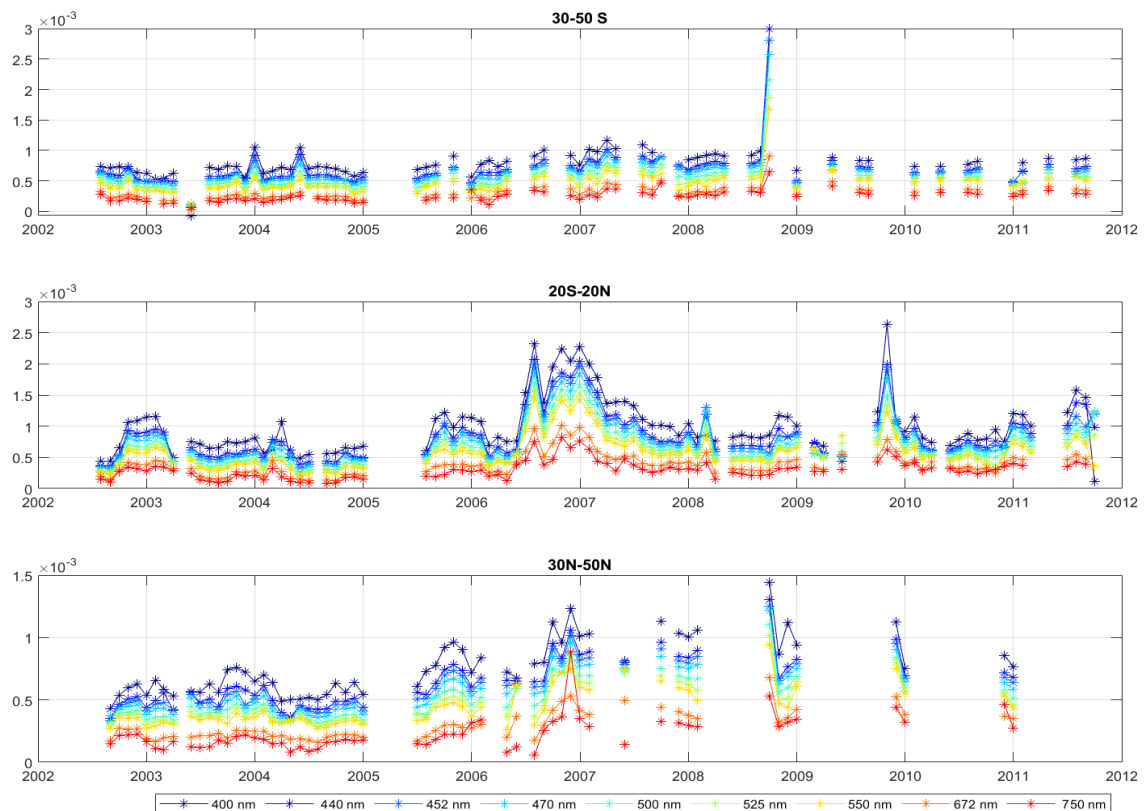


Figure 31. Time series of GOMOS-FMI aerosol extinction (1/km) at 20 km in the latitude zones 30-50 S (top), 20S-20N (center) and 30-50 N (bottom). The wavelengths are indicated in the figure legend.

We have plotted an analogous time series of aerosol extinction as shown in Figure 31, but using AERGOM data obtained from <https://cds.climate.copernicus.eu/cdsapp#!/dataset/10.24381/cds.239d815c?tab=form> . As it is seen in Figure 32, AERGOM aerosol extinction spectra have unrealistic shape after 2009. Furthermore, AERGOM often reports negative aerosol extinction at 440 nm and 750 nm, especially after 2009, and enhancements related to volcanic eruptions are less visible.

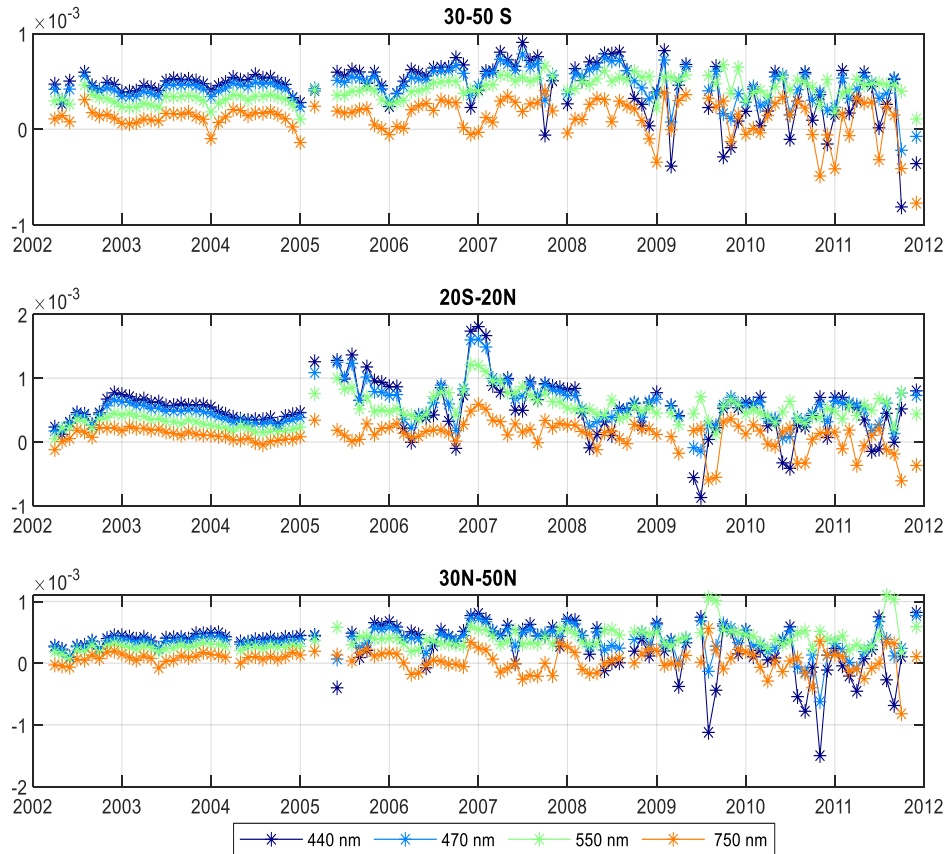


Figure 32. As Figure 31, but for AERGOM aerosol extinction.

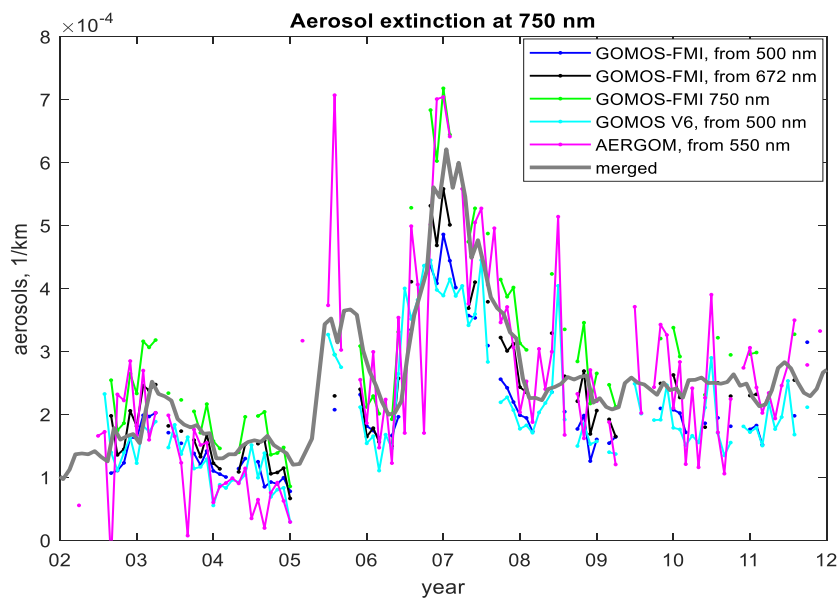


Figure 33. GOMOS aerosol extinction at 750 nm computed by different methods: GOMOS-FMI retrieved at 750 nm (green), GOMOS-FMI converted from 672 nm (black), GOMOS-FMI converted from 500 nm (blue), GOMOS IPF v6 converted from 500 nm (cyan) and AERGOM converted from 550 nm (magenta). Thick grey line indicates merged aerosol extinction. All time series are for the latitude bin 0-10°N and altitude 22 km.

To select the best dataset to be used in the merged time series, we compared the GOMOS aerosol extinction at 750 nm time series, which was computed by different methods: either retrieved at 750 nm or computed from other wavelengths using the assumption on a fixed particle size distribution. These time series, which are computed using GOMOS-FMI aerosols, IPF v6 and AERGOM, are presented in Figure 33. AERGOM data at 750 nm are too noisy, therefore they are not shown in Figure 33. We found that the best agreement with the merged aerosol extinction time series is for GOMOS-FMI aerosol extinction converted from 672 nm. This is used in the creation of merged CREST aerosol climate data record.

3.4.5 Conclusions

The aerosol retrieval algorithm from averaged transmittance spectra has been developed and applied to the GOMOS dataset. The retrieved aerosol extinction profiles show realistic wavelength dependence, and they are in a good agreement with other datasets.

The new processed dataset has a better quality (wavelength-dependence, agreement with other datasets, enhancements during volcanic eruptions).

For the merged aerosol extinction dataset at 750 nm, GOMOS-FMI aerosol extinction data at 672 nm is used. The transformation to 750 nm is performed using the Ångström exponent.

3.5 WP 5. CDR of stratospheric aerosols

3.5.1 Merged dataset of aerosol profiles

The datasets from individual satellite instruments were collected and gridded as monthly zonal means with 10° step in the latitude. The following instruments were considered: GOMOS, OMPS-LP, OSIRIS, SAGE II, SAGE III/ISS, SCIAMACHY. All data were converted to the wavelength of 750 nm. We finally have chosen this wavelength because the OSIRIS data set was selected as the reference one and this data set is available only at 750 nm. For the conversion of SAGE II data, the Ångström exponent calculated from 525 nm and 1020 nm data was used. GOMOS data were converted using the Ångström exponent based on 400 and 675 nm data. OMPS-LP data were converted using a fixed PSD assumption as no data providing the Ångström exponent for the entire measurement period of OMPS-LP are available.

Gridded time series from individual instruments were compared and methods to remove biases between the time series were analyzed. As the OSIRIS time series is the longest one, we use it as a reference to adjust all other instruments.

SCIAMACHY, OMPS-LP and GOMOS are adjusted as follows. First, deseasonalized anomalies are computed (seasonal cycle is estimated using volcanic free periods). Then, the seasonal cycle is scaled to OSIRIS seasonal cycle using robust linear regression and added to the deseasonalized anomalies. This procedure ensures that the scaling is performed properly even in cases where not full year is covered by OSIRIS data.

For SAGE II and SAGE III/ISS, the offset is computed as the median difference between OSIRIS and occultation aerosol data in volcanic free periods and added to data. The adjustment procedure works well, also in complicated cases.

The merged aerosol extinction coefficient time series is calculated as the median of the adjusted data from the individual instruments. Taking the median eliminates the influence of outliers that might be present in the individual datasets.

Illustrations of original, adjusted and merged datasets in several latitude zones are presented in Figures 34-39. These figures show that the adjustment procedure makes the datasets from individual datasets very close to each other in overlapping periods.

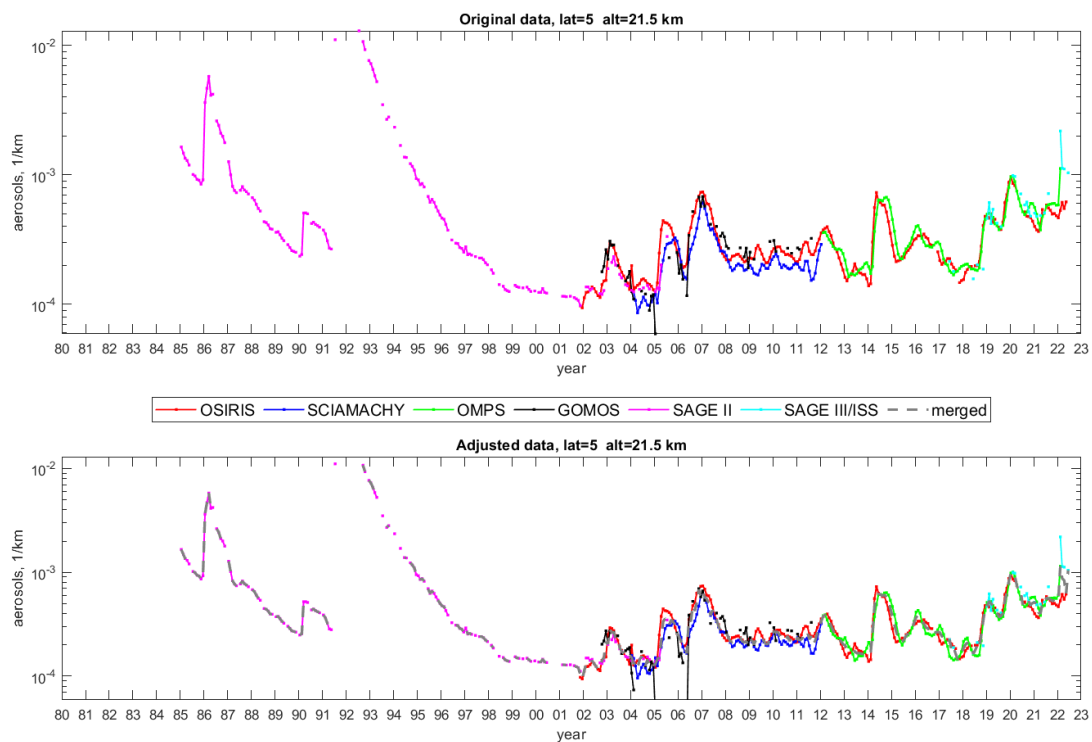


Figure 34. Aerosol extinction coefficient (1/km) at 21.5 km in the latitude zone 0-10°N. Colored lines correspond to aerosol records from individual instruments. Top panel: original data, bottom panel: adjusted data. The merged aerosol extinction coefficient is shown by grey line in the bottom panel.

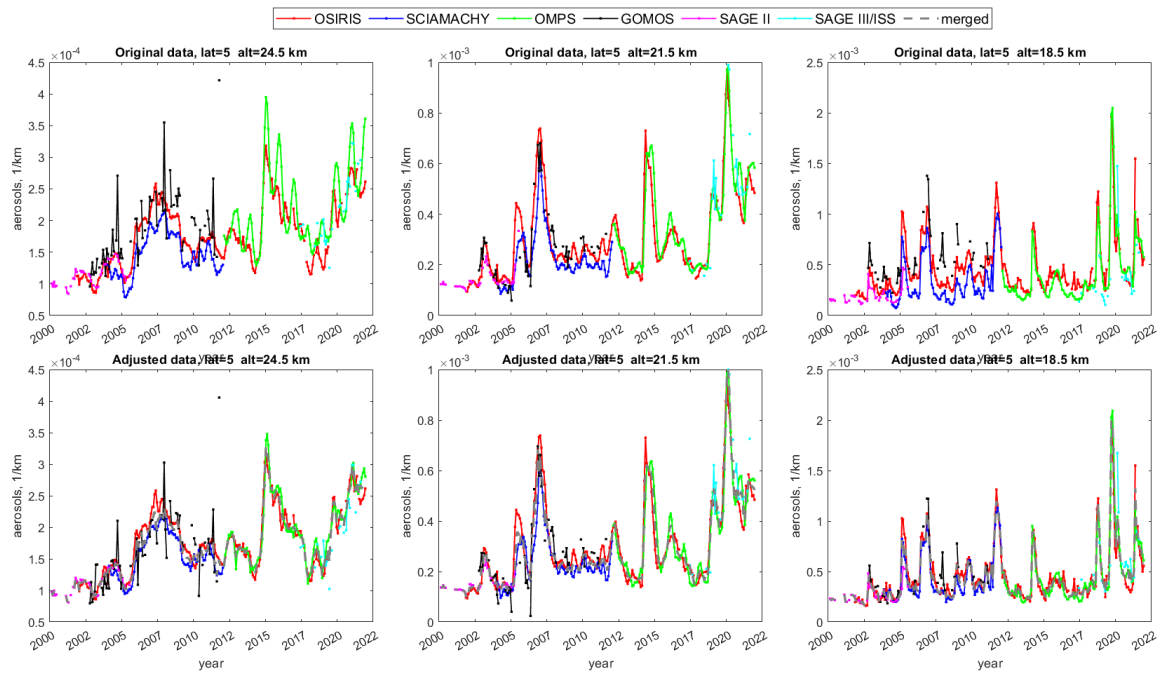


Figure 35. As Figure 34, but for several altitude levels and with the zoom on years 2000- 2021.

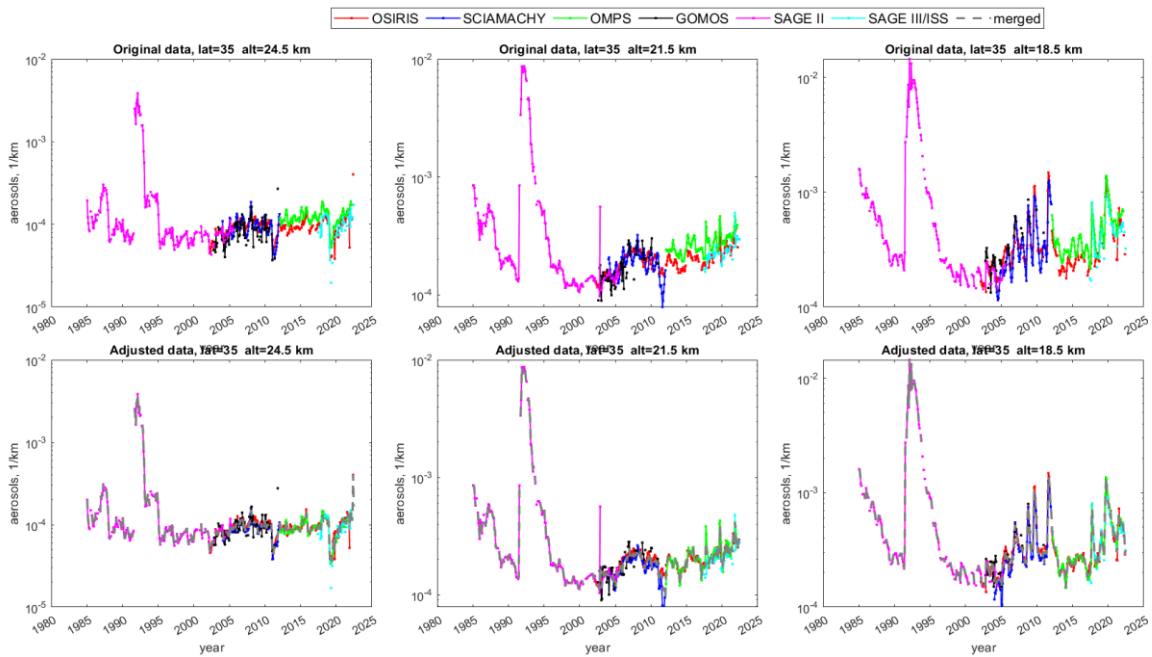


Figure 36. Original, adjusted, and merged aerosol extinction data in the subtropics (30°-40° N).

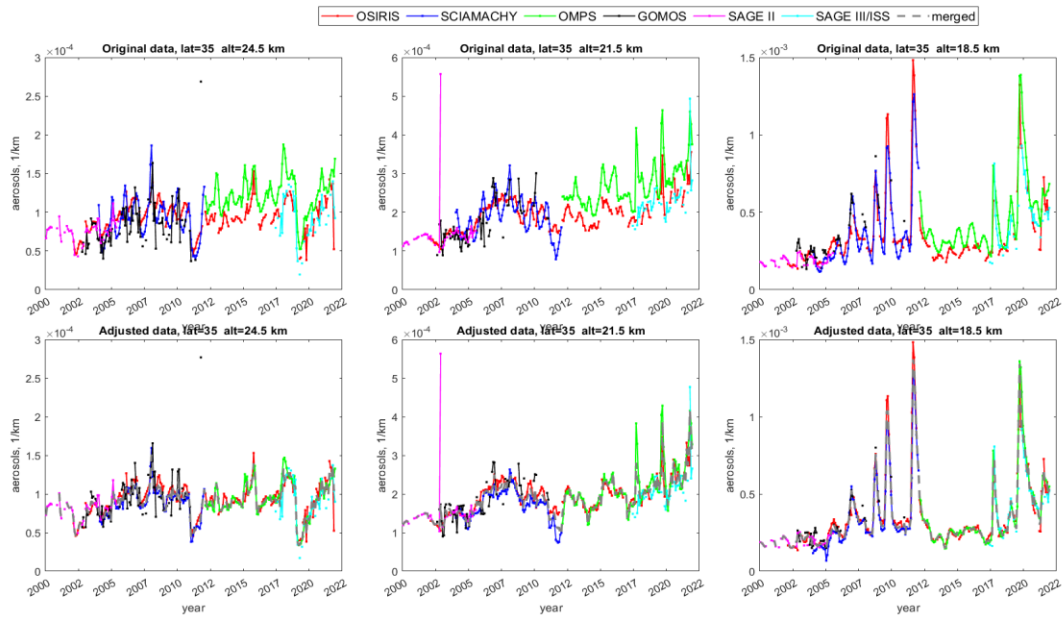


Figure 37. As Figure 36, but with the zoom on years 2000-2021

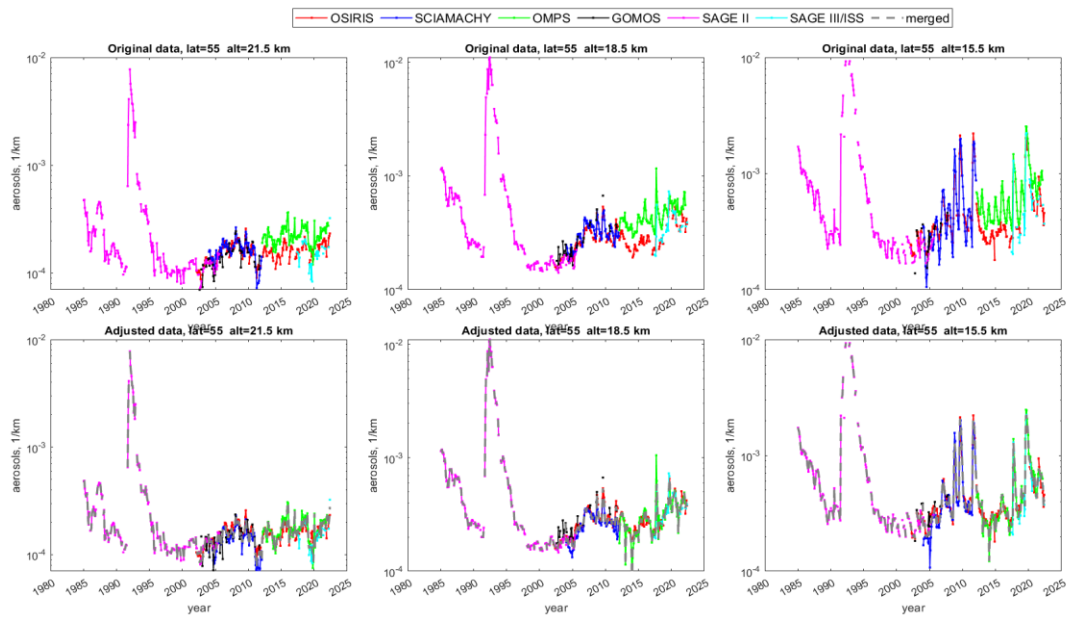


Figure 38. Original, adjusted, and merged aerosol extinction data at NH mid-latitudes (50°-60° N).

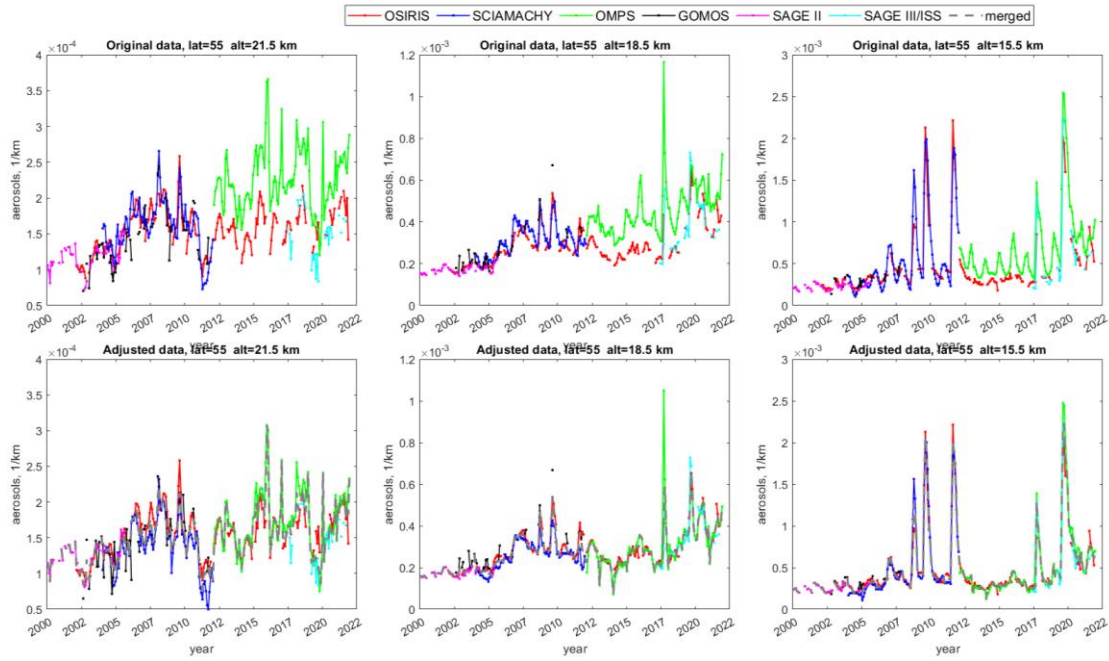


Figure 39. As Figure 38, but with the zoom on years 2000-2021

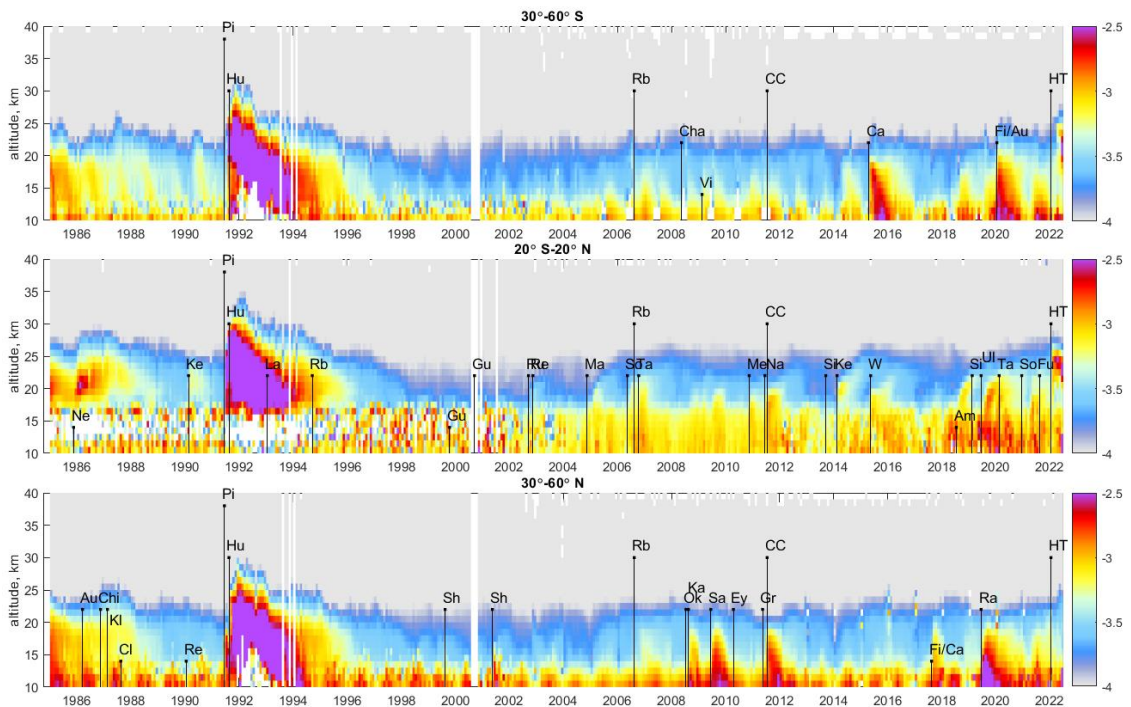


Figure 40. The CREST merged aerosol extinction profiles at 30°-60°S (top), 20°S-20°N (center) and 30°-60°N (bottom). The volcanos are indicated by black bars with the length proportional to volcanic explosivity index (VEI). Volcanos with VEI>=5 are shown for all latitude zones, and with

Figure 40 shows the aerosol extinction profiles from the merged CREST dataset in three latitude zones, 30°-60°S (top), 20°S-20°N (center) and 30°-60°N (bottom). The main volcanic

eruptions and strong wildfires are indicated in the figure with a bar of length proportional to the volcanic explosivity index (VEI). As observed in Figure 40, enhancements of aerosol extinction correspond to the enhanced volcanic activity or strong wildfires, which are listed in Table 1.

Table 1. The list of volcanic eruptions and strong wildfires.

year	month	Volcano/wildfire name	Abbreviation	Latitude (deg North)	VEI
1985	11	Nevado del Ruiz	Ne	5	3
1986	3	Augustine	Au	59	4
1986	11	Chikurachki	Chi	50	4
1987	2	Kliuchevskoi	Kl	56	4
1987	8	Cleveland	Cl	53	3
1990	1	Redoubt	Re	61	3
1990	2	Kelut	Ke	-8	4
1991	6	Pinatubo	Pi	15	6
1991	8	Mt.Hudson	Hu	-46	5
1993	1	Laskar	La	-23	4
1994	9	Rabaul	Rb	-4	4
1999	8	Sheveluch	Sh	57	4
2000	9	Guagua Pichincha	Gu	0	4
2001	5	Shiveluch	Sh	56	4
2002	9	Ruang	Ru	2	4
2002	11	Reventador	Re	0	4
2004	11	Manam	Ma	4	4
2006	5	Soufrière Hills	So	16	4
2006	8	Rabaul	Rb	-4	5
2006	10	Tavurvur	Ta	-4	4
2008	5	Chaitén	Cha	-42	4
2008	7	Okmok	Ok	55	4
2008	8	Kasatochi	Ka	55	4
2009	2	Fire/Victoria	Vi	-37	3
2009	6	Sarychev	Sa	48	4
2010	4	Eyjafjallajokull	Ey	64	4
2010	11	Merapi	Me	-8	4
2011	5	Grimsvótn	Gr	64	4
2011	6	Nabro	Na	13	4
2011	7	Cordon Caulle	CC	-40	5
2013	9	Sinabung	Si	3	4
2014	2	Kelut	Ke	-8	4
2015	4	Calbuco	Ca	-41	4
2015	5	Wolf	W	0	4
2017	8	Wildfires/California	Fi/Ca	51	3
2018	7	Ambae	Am	-15	3
2019	2	Sinabung	Si	3	4
2019	6	Ulawun	Ul	-5	4
2019	6	Raikoke	Ra	48	4
2020	2	Taal	Ta	14	4
2020	1	Fire/Australia	Fi/Au	-35	4
2020	12	Soufriere St.Vincent	So	13	4
2021	8	Fukutoku-Oka-no-Ba	Fu	24	4
2022	1	HungaTonga-Hunga	HT	-21	5

3.5.2 Filling gaps in SAGE II data during Pinatubo

It has been reported in several publications that SAGE II aerosol load is underestimated or missing in the lower stratosphere during Pinatubo volcanic eruption (Kovilakam et al., 2020; Sukhodolov et al., 2018). The reason is "saturation" in SAGE II data, i.e., there are no values larger than $\sim 0.012 \text{ km}^{-1}$.

The GLOSSAC dataset (Kovilakam et al., 2020; Thomason et al., 2018) uses experimentally scaled CLAES data at these times/locations.

We applied the following approach in the merged CREST dataset. In the period affected by Pinatubo volcanic eruption, i.e., from June 1991 and lasting 3 years, the aerosol extinction $\beta(t)$ as a function of time for each altitude level is fitted by the function

$$f(t) = a + b(1 - \exp(-t/\tau_1))\exp(-t/\tau_2), \quad (2)$$

where a , b , τ_1 and τ_2 are parameters to fit. The coefficient a is estimated as the mean over the period from January to May 1991, while other parameters are obtained via non-linear least-squares fitting by the Levenberg-Marquardt algorithm. As illustrated in Figure 41 (left), the aerosol peak associated with the Pinatubo eruption follow well the function (2), which describes the exponential growth and decay, for the cases where SAGE II data are not saturated (Figure 41 (left) is for 27.5 km). For lower altitudes (from the tropopause to the level 8 km above the tropopause), the data from 3 to 10 months after the Pinatubo eruption are not used in the fit, as illustrated in Figure 41 (right). The fitted aerosol peak during the strong Pinatubo load exceeds the maximal aerosol extinction value of $\sim 0.012 \text{ km}^{-1}$ reported by SAGE II.

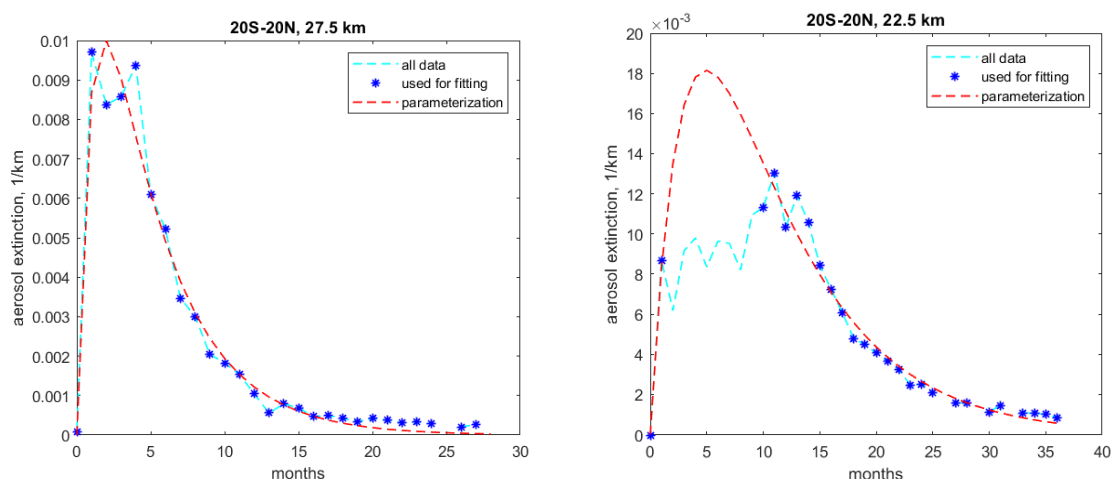


Figure 41. Example of the SAGE II aerosol fitting during the Pinatubo period with the function Eq.(1) at 27.5 km (left) and 22.5 km (right). The data are for latitudes 20°S-20°N.

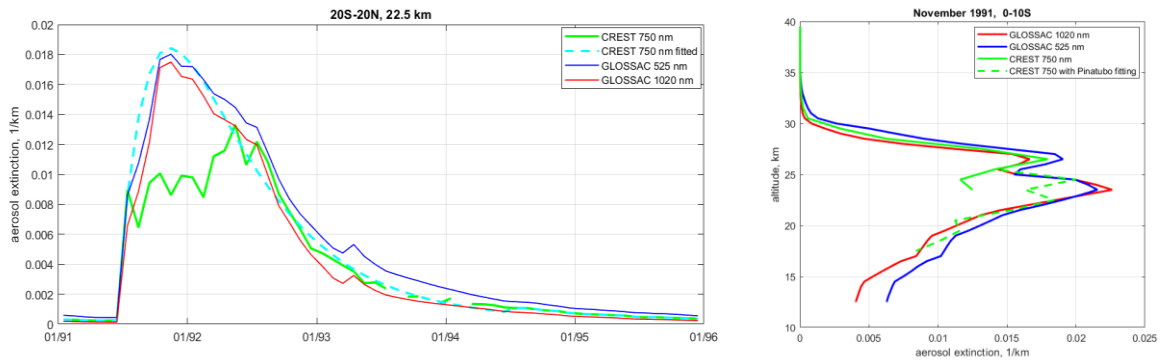


Figure 42. Left: time series of aerosol extinction at 22.5 km as reported by GLOSSAC (at 525 and 1020 nm) and CREST (original data (green solid line) and fitted by Eq. (2), green dashed line). Right: GLOSSAC, CREST original and Pinatubo-corrected aerosol profiles in November 1991, in the latitude zone 0° – 10° S.

We performed such Pinatubo-filtering to the data in the tropics (20° S – 20° N) and also in other latitude zones (20° – 40° , 40° – 60° , 60° – 90°), and found that the saturation affects primarily the data in the tropics. Therefore, for latitude zones from 20° S to 20° N the saturated aerosol data (i.e., for altitudes below 26 km, where the fitted aerosol value exceeds 0.011 km^{-1}) are replaced with the fitted values. Missing data during Pinatubo eruption are also replaced with the fit.

The resulting Pinatubo-corrected aerosol profiles are in good agreement with GLOSSAC, as illustrated in Figure 42.

3.5.3 Creating stratospheric aerosol optical depth (SAOD)

The stratospheric aerosol optical depth (SAOD) has been computed via integration of aerosol extinction profiles from tropopause to ~ 40 km. The resulting SAOD record is shown in Figure 43(a).

For using SAOD in climate simulations and in trend analyses, a gap-free dataset is needed. For this, we first replaced missing data for each latitude zone with 3-month smoothed values (Figure 43b). Then the triangulation method is applied to the time-latitude SAOD field, resulting in gap-free stratospheric aerosol climate data record, which is illustrated in Figure 43(c).

The global average (area-weighted) in the latitude range from 80° S to 80° N stratospheric aerosol optical depth is shown in Figure 43(d); it is used as aerosol proxy in WP6.

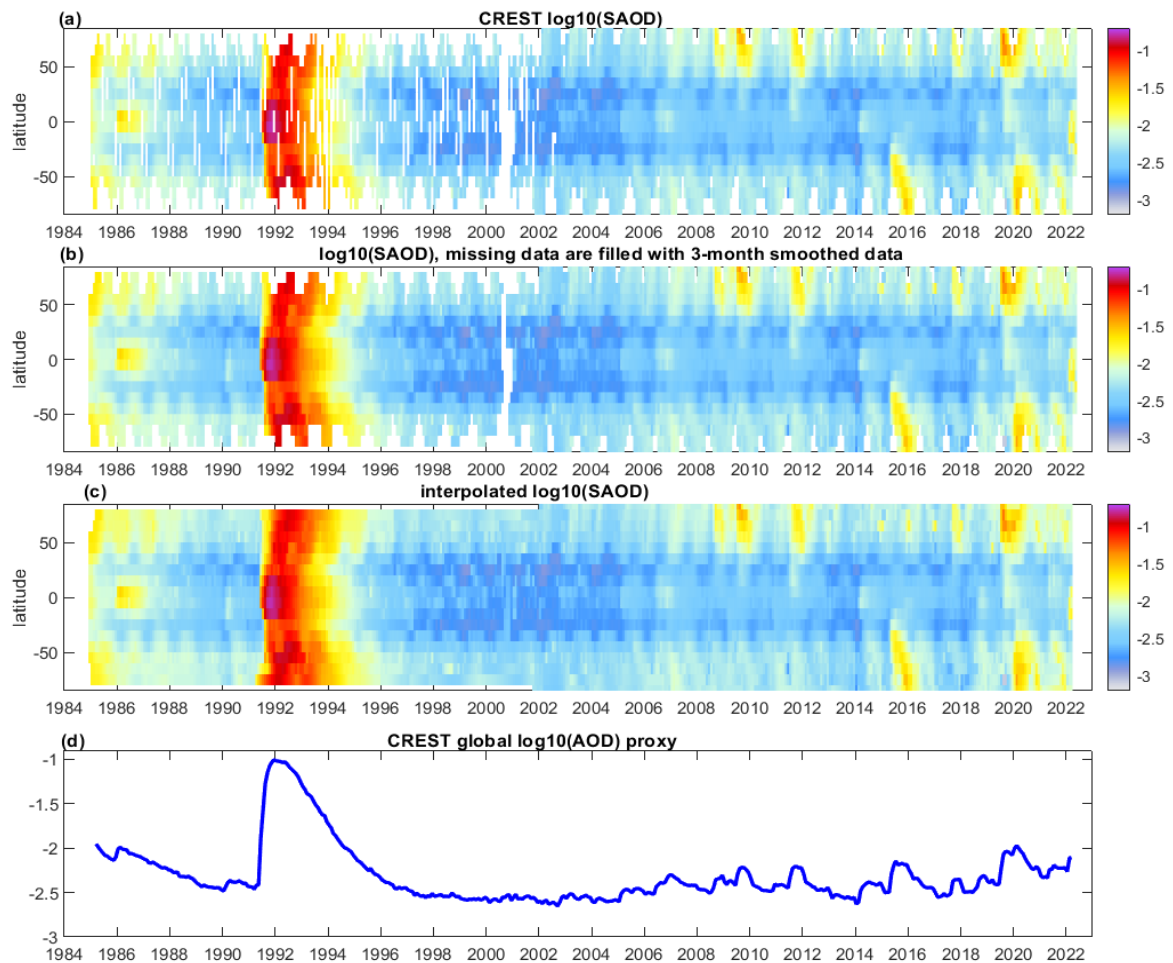


Figure 43. Illustration of creating CREST SAOD and aerosol proxy. (a) SAOD as obtained from integration of aerosol profiles; (b) as (a) but missing data are filled in with the 3-month mean, for each latitude zone; (c) the gap-free SAOD obtained from (b) by interpolation by Delaney triangulation; (d) global mean SAOD (aerosol proxy). All SAOD are presented in logarithmic scale.

3.5.4 The merged CREST SAOD dataset: illustrations, comparison with GLOSSAC

The interpolated CREST SAOD dataset is shown in Figure 44, together with main aerosol events (volcanic eruptions and wildfires), which are indicated by black circles of the size proportional to their volcanic explosivity index VEI (Table 1). As observed in Figure 44, aerosol enhancements correspond very well to volcanic eruptions and strong wildfires.

The comparison of CREST and GLOSSAC stratospheric optical depth datasets is shown in Figure 45. GLOSSAC provides SAOD at 525 nm and 1020 nm. The overall morphology of SAOD enhancements is very similar (taking into account the wavelength-dependence) in CREST and GLOSSAC. The comparison of global mean SAOD from CREST (750 nm) and GLOSSAC (525 nm and 1020 nm) is shown in Figure 46. CREST and GLOSSAC aerosol proxies are in very good agreement and show expected wavelength dependence of aerosols.

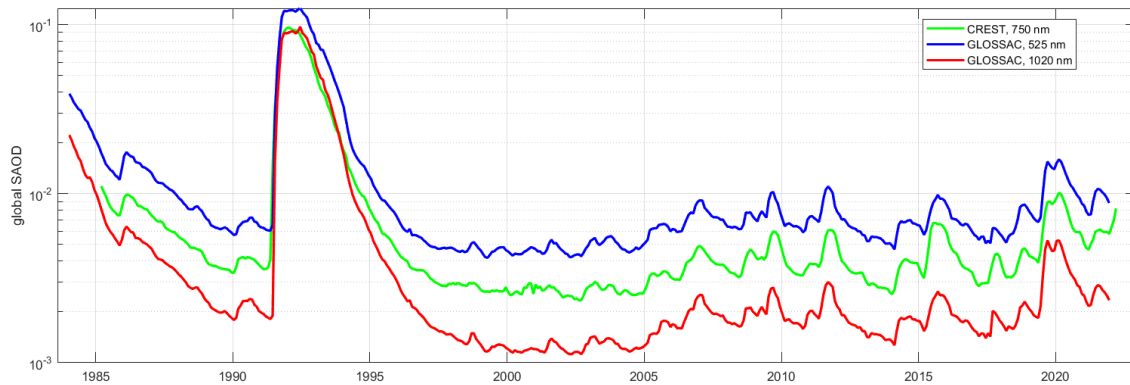


Figure 46. Global mean stratospheric optical depth from CREST (750 nm) and GLOSSAC (525 and 1020 nm).

The time series of monthly mean Ångström exponent α is provided with the CREST dataset. This allows transformation of the merged CREST AOD β_{750nm} to any desired wavelength λ (in nm) using the relation

$$\alpha = - \log \left(\frac{\beta(\lambda)}{\beta_{750nm}} \right) / \log \left(\frac{\lambda}{750} \right) \quad (3)$$

3.5.5 Summary

The climate data record of stratospheric aerosols (CREST) is created. It includes:

- Merged dataset of aerosol profiles at 750 nm from 8.5 to 39.5 km
- Merged dataset of stratospheric aerosol optical depth
- Global mean stratospheric optical depth, which can be used as aerosol proxy in trend analyses.

ESA-CREST is complementary to NASA-GLOSSAC. It provides aerosols at a different wavelength, 750 nm, and it uses a different collection of individual datasets included in the merged dataset. In addition, a different correction of saturated SAGE II data during Pinatubo period is applied in construction of the CREST dataset. The overall agreement of CREST and GLOSSAC is very good.

3.6 WP6. Application: influence of the volcanic activity on long-term ozone trends

To perform ozone trends sensitivity with new CREST aerosol optical depth proxy, SAGE-CCI-OMPS dataset of monthly deseasonalized anomalies developed in the framework of ESA Climate Change Initiative (Sofieva et al., 2017b) has been used.

Analysis have been done using a multiple linear regression technique, to separate the natural variability and long-term trends, i.e.,

$$O_3(t) = PWLT(t, t_0) + q_1 QBO_{30}(t) + q_2 QBO_{50}(t) + sF_{10.7}(t) + dENSO(t) + AOD(t), \quad (4)$$

where ozone trends are approximated with a piecewise linear function $PWLT(t, t_0)$ with the turnaround point in 1997, and $QBO_{30}(t) + q_2 QBO_{50}(t)$ are equatorial winds at 30 and 50 hPa, respectively (<http://www.cpc.ncep.noaa.gov/data/indices/>), $F_{10.7}(t)$ is the monthly average 10.7 cm solar radio flux (ftp://ftp.geolab.nrcan.gc.ca/data/solar_flux/monthly_averages/), and $ENSO(t)$ is the ENSO proxy (<http://www.esrl.noaa.gov/psd/enso/mei/table.html>). The ENSO index is used with 2 months lag, as done in several previous ozone trend analyses (e.g., Bourassa et al., 2014; Randel and Thompson, 2011; Sofieva et al., 2017b), and $AOD(t)$ is the aerosol optical depth. Two different aerosol optical depth dataset have been applied in this study, i.e., CREST aerosol optical depth at 750 nm and GLOSSAC aerosol optical depth at 525 nm. Autocorrelations were removed using the Cochrane–Orcutt transformation (Cochrane and Orcutt, 1949).

Figure 47 shows the latitude-altitude variation of linear trends in ozone (% dec⁻¹) calculated over 1985-1997 and 1997-2020 without aerosol optical depth (AOD) proxy (top panels), with GLOSSAC AOD (middle panels) and with CREST AOD (bottom panels). In general, the ozone trends exhibit similar behavior for all latitudes in the middle and upper stratosphere. The main differences are clearly visible in the tropical regions below about 25 km (Figure 48) for both considered periods of time, i.e., 1985-1997 and 1997-2020.

Note, that the ozone trends differences arise partially from the fact, that the stratospheric AODs are derived at different wavelengths for CREST (750 nm) and GLOSSAC (525 nm). To demonstrate the impact of the wavelength on the ozone trends variability, the differences between using GLOSSAC AOD at 525 and 1020 nm have been shown in Figure 49. The main differences follow the patterns presented in Figure 48 (right panels) and affect mainly the tropical regions below ~25 km for both considered periods of time, i.e., 1985-1997 and 1997-2020.

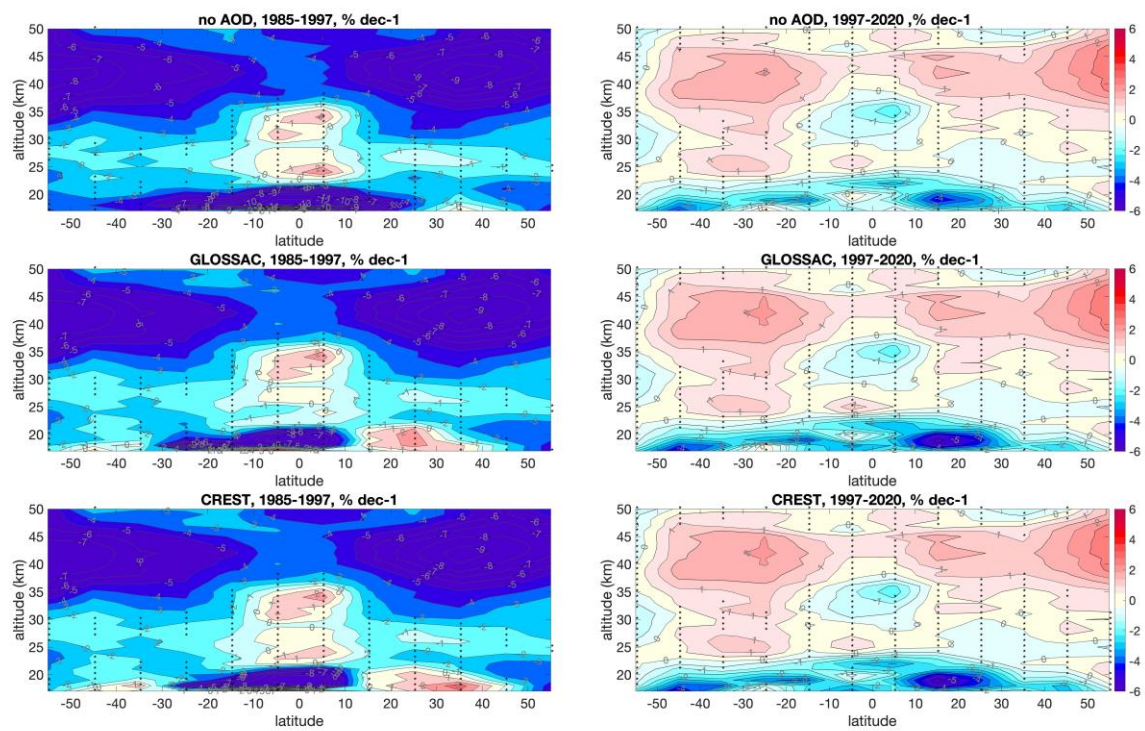


Figure 47. Latitude-altitude variation of linear trends in ozone ($\% \text{ dec}^{-1}$) calculated over 1985-1997 (left column) and 1997-2020 (right column). Top panels: ozone trends without AOD proxy, middle panels: ozone trends with GLOSSAC AOD at 525 nm, bottom panels: ozone trends with CREST AOD at 750 nm. The dotted areas denote trends that are statistically not significant.

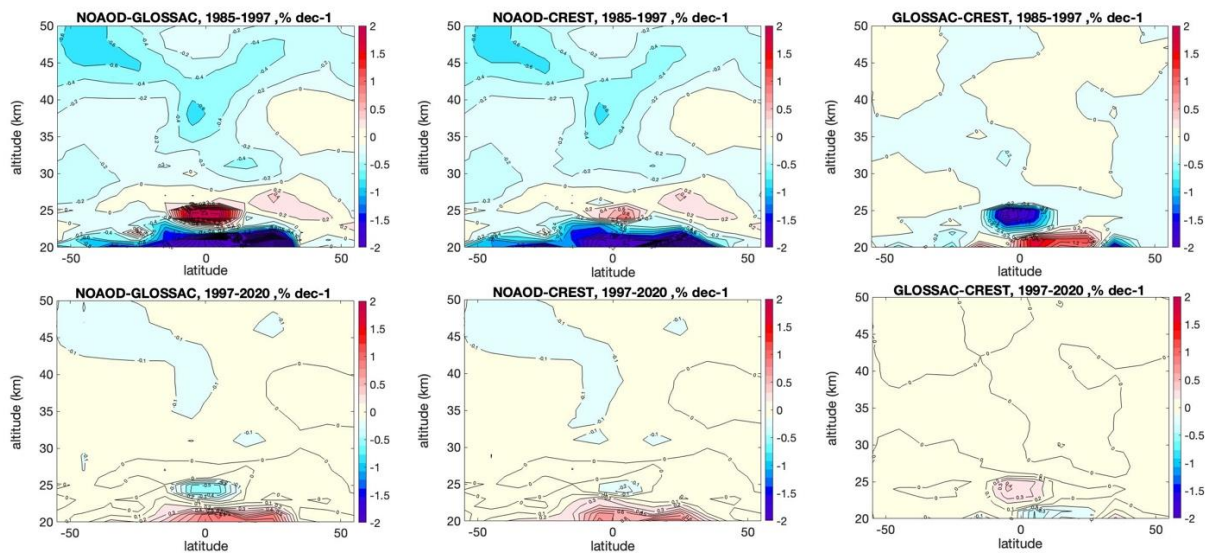


Figure 48. Latitude-altitude variation of linear trends in ozone ($\% \text{ dec}^{-1}$) calculated over 1985-1997 (upper panels) and 1997-2020 (bottom panels). Left column: the difference between ozone trends without AOD proxy and with GLOSSAC AOD. Middle column: the difference between ozone trends without AOD and with CREST AOD. Right column: the difference between ozone trends with GLOSSAC AOD and CREST AOD.

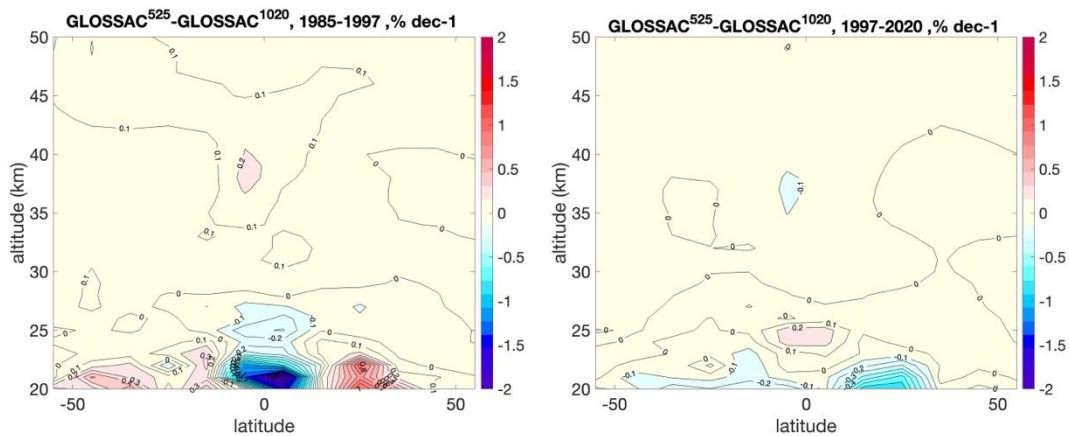


Figure 49 Latitude-altitude variation of linear trends in ozone (% dec⁻¹) calculated over 1985-1997 (left panel) and 1997-2020 (right panel). Both panels show the difference between ozone trends with GLOSSAC AOD at 525 nm and with GLOSSAC AOD at 1020 nm.

4 Datasets and data access

The merged CREST aerosol datasets are collected in one netcdf-4 dataset, which is available at <https://fmi.b2share.csc.fi/records/8bfa485de30840eba42d1d407f4ce19c>

The structure of the file ESA-CREST-v1.0-fv001.nc and variables are the following:

Format:

netcdf4_classic

Global Attributes:

title = 'Climate data records of stratospheric aerosols: merged aerosol extinction profiles and stratospheric optical depth'

summary = 'The merged datasets are created using aerosol data from SAGE II NASA-V7.00, OSIRIS USask-V7.2, SCIAMACHY UBr-V3.0, GOMOS FMI-v1.0, OMPS_LP UBr-V1.2, SAGE III/ISS NASA-V5.2'

comment = 'The datasets are for 750 nm. They are created in the framework of ESA project CREST <https://eo4society.esa.int/projects/crest/>. Definitions of parameters and data processing are described in the dedicated Technical Note'

number_of_altitude_levels = '32'

number_of_latitude_bins = '18'

geospatial_lat_resolution = '10 deg '

geospatial_lat_min = '-90 deg'

geospatial_lat_max = '90 deg'

geospatial_vertical_min = '8.5 km'

geospatial_vertical_max = '39.5 km'

value_for_nodata = 'NaN'

date_created = '20220926T213156'

creator_name = 'Viktoria Sofieva'

creator_email = 'viktoria.sofieva@fmi.fi'

address = 'P.O.Box 503, 00101 Helsinki, Finland'

Conventions = 'CF-1.8'

standard_name_vocabulary = 'NetCDF Climate and Forecast(CF) Metadata Convention version 18'

Dimensions:

time = 452

latitude_centers = 18

```

altitude      = 32
Variables:
time
  Size: 452x1
  Dimensions: time
  Datatype: double
  Attributes:
    units      = 'days since 1980-01-01 00:00:0.0'
    standard_name = 'time'
    calendar   = 'standard'
    comment    = 'one data point for each month: on the 15st of the month'
Year
  Size: 452x1
  Dimensions: time
  Datatype: single
Month
  Size: 452x1
  Dimensions: time
  Datatype: single
latitude_centers
  Size: 18x1
  Dimensions: latitude_centers
  Datatype: single
  Attributes:
    units      = 'degrees_north'
    standard_name = 'latitude'
    long_name  = 'centers of 10 deg latitude bins'
altitude
  Size: 32x1
  Dimensions: altitude
  Datatype: single
  Attributes:
    units      = 'km'
    standard_name = 'altitude'
    long_name  = 'geometric altitude'
merged_aerosol_extinction
  Size: 32x18x452
  Dimensions: altitude,latitude_centers,time
  Datatype: double
  Attributes:
    units      = '1/km'
    long_name  = 'merged profiles of aerosol extinction at 750 nm'
Pinatubo_fitting_flag
  Size: 32x18x452
  Dimensions: altitude,latitude_centers,time
  Datatype: single
  Attributes:
    unit      = 'dimensionless'
    Description = ' 1 - saturated SAGE II values are replaced by parameterized values, 0 - pure
experimental data '
SAOD
  Size: 18x452
  Dimensions: latitude_centers,time
  Datatype: double
  Attributes:
    units      = 'dimensionless'
    long_name  = 'stratospheric aerosol optical depth at 750 nm'

```

```

description = 'integrated aerosol profiles from tropopause to ~40 km'
SAOD_interpolated
Size: 18x452
Dimensions: latitude_centers,time
Datatype: double
Attributes:
  units = 'dimensionless'
  long_name = 'interpolated stratospheric aerosol optical depth at 750 nm'
  description = 'integrated aerosol profiles from tropopause to ~40 km and horizontally
interpolated '
Angstrom_exponent
Size: 18x452
Dimensions: latitude_centers,time
Datatype: double
Attributes:
  units = 'dimensionless'
  standart_name = 'angstrom_exponent_of_ambient_aerosol_in_air'
  description = 'Angström exponent for transformation of the dataset to other wavelengths
according to the formula: AE = - log(ext_wl/ext_750nm)/log(wl/750)'
Global_SAOD
Size: 452x1
Dimensions: time
Datatype: double
Attributes:
  units = 'dimensionless'
  long_name = 'global stratospheric aerosol optical depth at 750 nm'
  description = 'area-weighted global mean stratospheric aerosol optical depth at 750 nm'

```

5 Main results and useful future work

The main result of the CREST project is the created aerosol climate data records, which covers the period from 1984 to 2022. The CREST dataset includes:

- Merged dataset of aerosol extinction profiles
- Merged dataset of stratospheric aerosol optical depth
- Merged global stratospheric aerosol optical depth time series (aerosol proxy)

The ESA-CREST aerosol dataset is complementary to NASA-GLOSSAC, and it provides valuable information about the long-term changes and variability of stratospheric aerosols. The created dataset can be used as a proxy in various trend analyses of climate-change related studies.

In addition, we improved aerosol dataset from individual instruments. New GOMOS multi-wavelengths monthly averaged aerosol profile dataset (FMI-GOMOSaero) has been created. The SCIAMACHY and OMPS-LP aerosol extinction profile retrievals of UBr have been improved and the new versions of the aerosol datasets have been produced.

The CREST dataset can be useful for other activities. In particular, it can be included in the Aerosol_CCI and in C3S. It is worth to extend regularly the CREST aerosol datasets in the

future. When ALTIUS aerosol data are available, they can be included in the merged CREST dataset.

Possible other future activities might include:

- Creating merged gridded (i.e., with resolved longitudinal structure) stratospheric aerosol dataset. Such dataset can be useful for various event studies
- Aerosol-cloud interaction and characterization, aerosol-cloud discrimination, cloud filtering
- Inclusion of the information about the tropopause height in the data binning procedure.
- Further improvement of the quality of the underlying aerosol datasets.
- Regular maintaining/extension of the merged aerosol dataset
- Inclusion of new datasets when available.

References

Bourassa, A. E., Rieger, L. A., Lloyd, N. D., and Degenstein, D. A.: Odin-OSIRIS stratospheric aerosol data product and SAGE III intercomparison, *Atmospheric Chemistry and Physics*, 12, 605–614, <https://doi.org/10.5194/acp-12-605-2012>, 2012.

Bourassa, A. E., Degenstein, D. A., Randel, W. J., Zawodny, J. M., Kyrölä, E., McLinden, C. A., Sioris, C. E., and Roth, C. Z.: Trends in stratospheric ozone derived from merged SAGE II and Odin-OSIRIS satellite observations, *Atmospheric Chemistry and Physics*, 14, 6983–6994, <https://doi.org/10.5194/acp-14-6983-2014>, 2014.

Cochrane, D. and Orcutt, G. H.: Application of Least Squares Regression to Relationships Containing Auto-Correlated Error Terms, *Journal of the American Statistical Association*, 44, 32–61, <https://doi.org/10.1080/01621459.1949.10483290>, 1949.

Kovilakam, M., Thomason, L. W., Ernest, N., Rieger, L., Bourassa, A., and Millán, L.: The Global Space-based Stratospheric Aerosol Climatology (version 2.0): 1979–2018, *Earth Syst. Sci. Data*, 12, 2607–2634, <https://doi.org/10.5194/essd-12-2607-2020>, 2020.

Kyrölä, E., Tamminen, J., Sofieva, V. F., Bertaux, J.-L., Hauchecorne, A., Dalaudier, F., Fussen, D., Vanhellemont, F., Fanton D’Andon, O., Barrot, G., Guirlet, M., Mangin, A., Blanot, L., Fehr, T., de Miguel, L., and Fraise, R.: Retrieval of atmospheric parameters from GOMOS data, *Atmos. Chem. Phys.*, 10, 11881–11903, <https://doi.org/10.5194/acp-10-11881-2010>, 2010.

Malinina, E., Rozanov, A., Rozanov, V., Liebing, P., Bovensmann, H., and Burrows, J. P.: Aerosol particle size distribution in the stratosphere retrieved from SCIAMACHY limb measurements, *Atmospheric Measurement Techniques*, 11, 2085–2100, <https://doi.org/10.5194/amt-11-2085-2018>, 2018.

Malinina, E., Rozanov, A., Niemeier, U., Wallis, S., Arosio, C., Wrana, F., Timmreck, C., Savigny, C. von, and Burrows, J. P.: Changes in stratospheric aerosol extinction coefficient

after the 2018 Ambae eruption as seen by OMPS-LP and MAECHAM5-HAM, *Atmospheric Chemistry and Physics*, 21, 14871–14891, <https://doi.org/10.5194/acp-21-14871-2021>, 2021.

Randel, W. J. and Thompson, A. M.: Interannual variability and trends in tropical ozone derived from SAGE II satellite data and SHADOZ ozonesondes, *Journal of Geophysical Research: Atmospheres*, 116, <https://doi.org/10.1029/2010JD015195>, 2011.

Santer, B. D., Bonfils, C., Painter, J. F., Zelinka, M. D., Mears, C., Solomon, S., Schmidt, G. A., Fyfe, J. C., Cole, J. N. S., Nazarenko, L., Taylor, K. E., and Wentz, F. J.: Volcanic contribution to decadal changes in tropospheric temperature, *Nature Geosci*, 7, 185–189, 2014.

Sofieva, V. F., Tamminen, J., Haario, H., Kyrölä, E., and Lehtinen, M.: Ozone profile smoothness as a priori information in the inversion from limb measurements, *Ann. Geophysicae*, 22, 3411–3420, 2004.

Sofieva, V. F., Ialongo, I., Hakkarainen, J., Kyrölä, E., Tamminen, J., Laine, M., Hubert, D., Hauchecorne, A., Dalaudier, F., Bertaux, J.-L., Fussen, D., Blanot, L., Barrot, G., and Dehn, A.: Improved GOMOS/Envisat ozone retrievals in the upper troposphere and the lower stratosphere, *Atmospheric Measurement Techniques*, 10, 231–246, <https://doi.org/10.5194/amt-10-231-2017>, 2017a.

Sofieva, V. F., Kyrölä, E., Laine, M., Tamminen, J., Degenstein, D., Bourassa, A., Roth, C., Zawada, D., Weber, M., Rozanov, A., Rahpoe, N., Stiller, G., Laeng, A., Clarmann, T. von, Walker, K. A., Sheese, P., Hubert, D., Roozendael, M. van, Zehner, C., Damadeo, R., Zawodny, J., Kramarova, N., and Bhartia, P. K.: Merged SAGE II, Ozone_cci and OMPS ozone profile dataset and evaluation of ozone trends in the stratosphere, *Atmospheric Chemistry and Physics*, 17, 12533–12552, <https://doi.org/10.5194/acp-17-12533-2017>, 2017b.

Solomon, S., Daniel, J. S., Neely, R. R., Vernier, J.-P., Dutton, E. G., and Thomason, L. W.: The Persistently Variable “Background” Stratospheric Aerosol Layer and Global Climate Change, *Science*, 333, 866–870, <https://doi.org/10.1126/science.1206027>, 2011.

Sukhodolov, T., Sheng, J.-X., Feinberg, A., Luo, B.-P., Peter, T., Revell, L., Stenke, A., Weisenstein, D. K., and Rozanov, E.: Stratospheric aerosol evolution after Pinatubo simulated with a coupled size-resolved aerosol–chemistry–climate model, *SOCOL-AERv1.0*, *Geosci. Model Dev.*, 11, 2633–2647, <https://doi.org/10.5194/gmd-11-2633-2018>, 2018.

Thomason, L. W., Ernest, N., Millán, L., Rieger, L., Bourassa, A., Vernier, J.-P., Manney, G., Luo, B., Arfeuille, F., and Peter, T.: A global space-based stratospheric aerosol climatology: 1979–2016, *Earth System Science Data*, 10, 469–492, <https://doi.org/10.5194/essd-10-469-2018>, 2018.

Vanhellemont, F., Matshvili, N., Blanot, L., Robert, C. É., Bingen, C., Sofieva, V. F., Dalaudier, F., Tétard, C., Fussen, D., Dekemper, E., Kyrölä, E., Laine, M., Tamminen, J., and Zehner, C.: AerGOM, an improved algorithm for stratospheric aerosol extinction retrieval from GOMOS observations – Part 1: Algorithm description, *Atmospheric Measurement Techniques*, 9, 4687–4700, <https://doi.org/10.5194/amt-9-4687-2016>, 2016.

Vernier, J.-P., Thomason, L. W., Pommereau, J.-P., Bourassa, A., Pelon, J., Garnier, A., Hauchecorne, A., Blanot, L., Trepte, C., Degenstein, D., and Vargas, F.: Major influence of tropical volcanic eruptions on the stratospheric aerosol layer during the last decade, *Geophysical Research Letters*, 38, <https://doi.org/10.1029/2011GL047563>, 2011.